Kinetics and Catalysis, Vol. 43, No. 5, 2002, pp. 603–638. Translated from Kinetika i Kataliz, Vol. 43, No. 5, 2002, pp. 645–683.

Desorption Dynamics of the Products of Heterogeneous Catalytic Reactions

M. U. Kislyuk

Semenov Institute of Chemical Physics, Russian Academy of Sciences, Moscow, 117977 Russia

Received January 10, 2002

Abstract—A review of experimental data on the desorption of excited molecules that are the products of heterogeneous catalytic reactions is given. It is shown that the sharply peaked spatial distributions of desorption flows (SDDFs) are observed in many systems. The translational energies of the products (T_{tr}) are much higher than the surface temperatures. A correlation of SDDF parameters and T_{tr} is found. The excitation of internal degrees of freedom (vibrations and rotations) is weaker. The vibrational and rotational temperatures (T_{vib} and T_{rot}) obey the following inequalities: $T_{tr} > T_{vib} > T_{rot}$ or $T_{tr} \geq T_{vib} > T_{rot}$, and $T_{rot} \approx T_{surf}$. Models for the description of the desorption of excited molecules are considered. New data on the active sites for anisotropic and stepped surfaces, from which desorption occurs, are discussed.

INTRODUCTION

In 1968, van Willigen published a paper [1] describing the spatial distribution of desorbing hydrogen molecules diffusing through flat metallic membranes. This distribution was sharply peaked along the normal to the surface. He proposed a model based on the principle of microscopic reversibility to explain this phenomenon by the excitation of the translational degree of freedom along the surface normal. That paper stimulated further studies of desorption dynamics.

It was assumed earlier that the temperature of desorbing molecules is equal to the temperature of a surface. The sharply peaked spatial distributions of the desorption flow (SDDF) of molecules suggest that these molecules have excessive translational energy; that is, there is repulsion of molecules from the surface. This was first confirmed by Dabiri *et al*. [2], who carried out direct measurements of the velocities of desorbing hydrogen molecules, and by researchers in other laboratories for other systems [3–10].

Further attempts were made [11–13] to detect anisotropic SDDF on anisotropic surfaces. However, early attempts failed probably because those studies concerned hydrogen desorption.

In 1989–1990, Matsushima detected SDDF anisotropy [14] and the so-called collimated (directed at a certain angle to the surface) desorption of CO_2 molecules [15] formed in CO oxidation on Pd(110) and Pt(110) surfaces. These studies made it possible to determine the localization of active sites and their symmetries.

Several processes of the Langmuir–Hinshelwood type are known that are accompanied by the emission of translationally excited molecules: $2H_{ads} \longrightarrow H_2$, $2N_{ads} \longrightarrow N_2$, $N_{ads} + O_{ads} \longrightarrow NO$, $C_{ads} + O_{ads} \longrightarrow CO$, $CO_{ads} + O_{ads} \longrightarrow CO_2$, $CH_{3,\,ads} + H_{ads} \longrightarrow CH_4$, and $N_2O_{ads} \longrightarrow N_2 + O_{ads}$. All these reactions, except for the last one, are recombinative desorption processes. The reverse processes (dissociative chemisorption) occur with high activation energies.

Of course, no information can be obtained if molecules stick to the surface after their formation and are thermolyzed. Unfortunately, many processes behave in this way.

The use of modern spectroscopic methods based on laser-induced fluorescence (LIF), resonance-enhanced multiphoton ionization (REMI), electron-induced fluorescence (EIF), and others made it possible to measure the excitation of the internal degrees of freedom of desorbing molecules.

Recently, the results of SDDF measurements and the excitation of the internal degrees of freedom of the molecules formed by the Eley–Rideal mechanism [6, 16, 17] were published.

Analysis of the excited states of molecules leaving the surface provide information on the dynamics of an elementary act that precedes desorption and, in some cases, information on the active sites for the reaction.

1. EXPERIMENTAL METHODS

For SDDF measurements, desorbed molecules should be detected at different angles of their emission from the surface. For carrying out a heterogeneous process, various methods are used: reactant supply onto the surface by their diffusion through metallic membranes (DMM), molecular beams (MB), temperature-programmed desorption/reaction (TPD/TPR), steady-state catalytic reaction (SSCR), and others.

The first of these methods was widely used to study the desorption dynamics of hydrogen, which readily penetrates through membranes at high temperatures

0023-1584/02/4305-0603$27.00

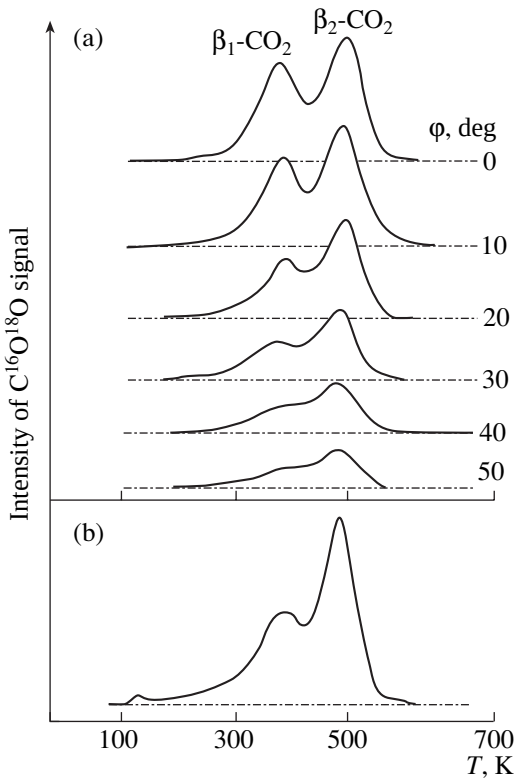

Fig. 1. Space-resolved TPR spectra for CO oxidation on Rh(111) (a) observed at different angles (φ, deg) to the surface normal and (b) the integral spectrum [20].

[18]. In this case, a rather intense desorption flow can be obtained, making it possible to accumulate the signal and measure SDDF, the velocities of molecules, and distributions over the internal degrees of freedom. Earlier, this method was only applied to hydrogen, but it can be extended to oxygen on silver and carbon monoxide on iron.

Modulated molecular beams were used to study the kinetics and dynamics of fast heterogeneous processes [19]. This method was applied to SDDFs of CO_2, H_2O, HD, and other molecules, although the surface concentrations of these reactants under these conditions remain unmeasured. This uncertainty is due to the interruption of the incident beam. Therefore, this method fails to detect the "kinetic transition" (a drastic change in the process rate given certain concentrations of reactants), which is characteristic of CO oxidation on platinum-group metals.

Rettner and coworkers were the first to use beams of atomic hydrogen for SDDF measurements of products in Eley–Rideal reactions: $H + Cl_{ads} \longrightarrow HCl$ [6], $H + D_{ads} \longrightarrow HD$, $D + H_{ads} \longrightarrow HD$ [16], $H + CHCH_{3,\,ads} \longrightarrow CH_4$, $D + CD_{3,\,ads} \longrightarrow CD_4$ [17]. The advantages of this method are the existence of a certain momentum parallel to the surface and the high potential energy of atoms resulting in sharply peaked SDDFs. The first of these factors is very useful for the elucidation of the reaction mechanism.

Space-resolved TPD/TPR methods are widely used for SDDF measurements because they are applicable to the processes with Langmuir–Hinshelwood mechanisms over a wide range of temperatures and surface concentrations.

Typical TPR spectra with the spatial resolution of CO_2 formed in the reaction of CO oxidation on Rh(111) at different emission angles are shown in Fig. 1a together with the integral spectrum (Fig. 1b) [20]. It is seen from this figure that the β_1-form peak in the integral spectrum is much lower than for β_2, but it has about the same height if desorption is measured along the normal to the surface. This means that the SDDF of β_1 form is more sharply peaked along the normal than the SDDF of β_2 form. SDDF parameters can easily be obtained by analyzing the spectra registered at different angles of molecule emission.

More recently, Matsushima and coworkers [21] supplemented this method with the measurements of the velocities of desorbing molecules using an desorption beam chopper with cross-correlation. Figure 2 shows the schematic of this setup. It consists of three independently evacuated chambers. The main chamber is a standard ultrahigh vacuum system equipped with instruments for LEED and XPS analyses, a quadrupole mass spectrometer, argon gun, and a gas inlet. A monocrystalline sample is mounted on the manipulator that allows one to vary the angle relative to the surface normal for desorption measurements. The chopper is in an intermediate chamber with windows connecting it with the main chamber and with a measuring chamber. The latter contains a high-sensitivity mass spectrometer working in a pulse-count regime. To provide high rates of CO_2 and H_2O evacuation, cryogen panels are used in the intermediate and measuring chambers.

In addition to the above-mentioned advantages, the TPD/TPR method has some limitations. Experiments are carried out in the regime of temperature increase accompanied by decreasing surface coverage, which can in turn lead to surface reconstruction. Thus, the apparent features may include dependences on the reactant concentrations, temperature, and surface structure.

Recently, SDDF measurements were carried out in the regime of a steady state process. This became possible due to modifications in apparatus by using the systems with a high pumping rate and some other units [22].

The above overview of the methods is very short. For more detailed information on SDDF measurements, see the review paper by Comsa and David [23].

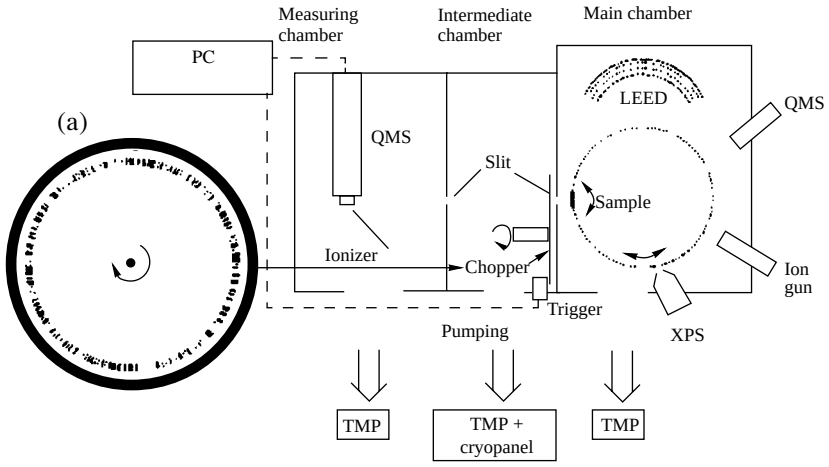

Fig. 2. Schematic of a setup for SDDF measurements and the measurements of the velocities of desorbing molecules [21]: the insert (a) shows the configuration of the chopper disk, LEED is the low-energy electron diffractometer, QMS is the quadrupole mass spectroscopy, XPS is the X-ray photoelectron spectrometer, TMP is a turbomolecular pump.

2. MAIN FEATURES AND MODELS DESCRIBING SPATIAL AND ENERGY DISTRIBUTIONS OF DESORBING MOLECULES

2.1. One-Dimensional Model and Spatial Distributions

Van Willigen [1] derived the following equation based on the principle of microscopic reversibility:

$$I/I_0 = [(\varepsilon + \cos^2\varphi)\exp(-\varepsilon\tan^2\varphi)]/[(\varepsilon + 1)\cos\varphi], \quad (1)$$

where I_0 and I are the intensities of a desorption flow along the normal to the surface and at angle φ to the normal, respectively; $\varepsilon = E_a/kT_{surf}$ is the activation energy of adsorption; k is the Boltzmann constant; and T_{surf} is the surface temperature.

Note that this equation transforms into the well-known Knudsen equation at $\varepsilon = 0$:

$$I/I_0 = \cos\varphi, \quad (2)$$

which is correct for evaporation and nonactivated adsorption.

The following simple empirical equation is frequently used for SDDF description:

$$I/I_0 = \cos^n\varphi. \quad (3)$$

This is a rather accurate approximation of Eq. (1), especially for high values of n. As we showed in [24], there is a simple expression relating n and ε, as illustrated in Figs. 3 and 4:

$$n \approx 2\varepsilon + 1. \quad (4)$$

From now on, we will use Eq. (3) and other similar formulas to describe the SDDFs of gases and analyze the regularities, because these formulas are simple and clear.

The relationship between E_a and n is easy to obtain from Eq. (4):

$$E_a \approx kT_{surf}(n-1)/2. \quad (5)$$

Comsa and David [25] found that the following equation provides a more correct description of SDDF:

$$I/I_0 = (1-a) \times \{[(\varepsilon + \cos^2\varphi)\exp(-\varepsilon\tan^2\varphi)]/[(\varepsilon + 1)\cos\varphi]\} + a\cos\varphi \quad (6)$$

or, in a simpler form;

$$I/I_0 = (1-a)\cos^n\varphi + a\cos\varphi. \quad (7)$$

These equations were obtained by summing Eqs. (1) and (2) or (3) and (2) with coefficients $(1-a)$ and a that characterize the contributions of the sharply peaked distribution and the cosine Knudsen distribution to the flow intensity along the normal to the surface. The typical example of the observed distribution [26] described by this model is shown in Fig. 5.

Van Willigen and Comsa's models use the classical Lennard-Jones' understanding of the activated dissociative chemisorption of gases. The one-dimensional potential of the interaction of molecule AB with the surface is shown in Fig. 6 as a combination of two curves corresponding to the molecular and dissociative adsorption. The resulting potential energy curve has two maxima separated by an activation barrier (point X). If the top of the barrier is above the ground state of molecule AB in the gas phase, adsorption is activated. In the case of desorption (when the molecule moves from point X to infinity), the molecule acquires excessive translational energy. If the desorbing molecule is trapped in a potential well corresponding to the molecular state after overcoming the potential barrier, then it loses excess energy and desorbs with a thermal velocity according to the Knudsen law.

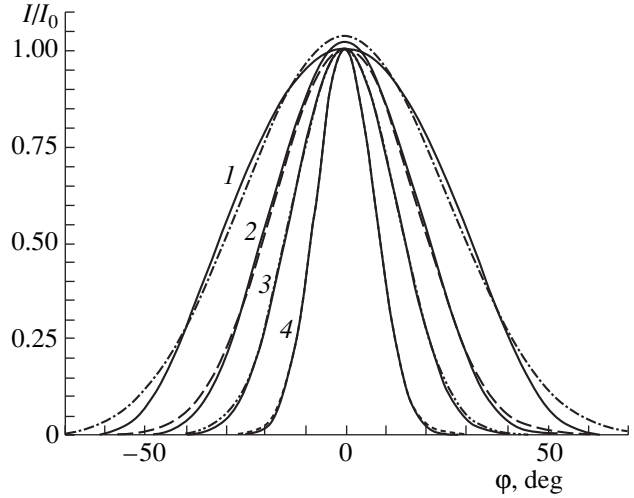

Fig. 3. Curves described by van Willigen equation (1) at different values of parameter $\varepsilon = E_a/kT$ (solid lines) and their approximation by empirical functions of the $\sigma\cos^n\varphi$ form (dashed line): (*1*) $\varepsilon = 2$, $n = 4.9$; (*2*) $\varepsilon = 5$, $n = 10.8$; (*3*) $\varepsilon = 10$, $n = 20.7$; and (*4*) $\varepsilon = 30$, $n = 60.8$.

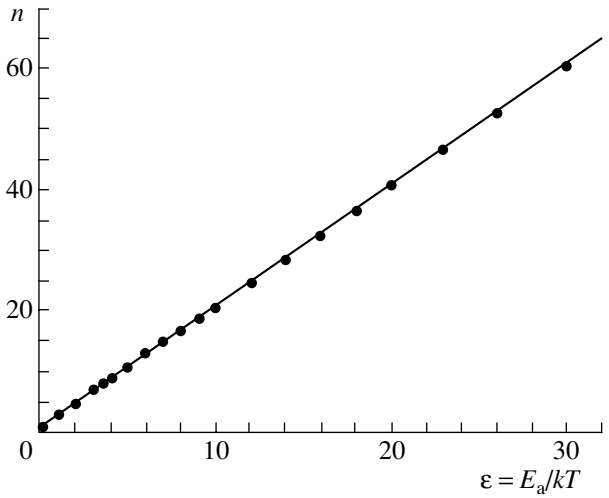

Fig. 4. Dependence of n on $\varepsilon = E_a/kT$ calculated from the approximation of Eq. (1) by empirical functions of the $\sigma\cos^n\varphi$ form (points) and the linear dependence $n = 2\varepsilon + 1$ (line) [24].

Equations (1) and (6) correctly describe SDDF from flat isotropic surfaces, but the one-dimensional model contradicts experimental measurements of the molecule velocities desorbed at different angles to the surface normal [23] and to some estimates of E_a [11, 12, 27–29], as will be seen from further discussion.

This model accommodates three main assumptions: the principle of microscopic reversibility, the one-dimensional potential, and the consideration of only translational energy, whereas other degrees of freedom of desorbing molecules are neglected. The two latter assumptions lead to considerable disagreement between the model and experiments. It has recently been shown that E_a depends on the internal degrees of freedom, especially on the vibrational energy [30]. Moreover, many examples of anisotropic and inclined SDDFs were found.

Nevertheless, the one-dimensional model is often used in estimating E_a because there are no experimental or theoretical data on the dependences of the excitation of internal degrees of freedom on the angle of molecule desorption from the surface, and SDDFs and molecule distribution over velocities are assumed to be dependent on E_a.

Numerous data have been obtained from measurements of SDDFs and molecule velocities on various isotropic surfaces. The desorption of CO_2 as a product of CO oxidation has been studied in most detail. Many papers have been devoted to the desorption of hydrogen and nitrogen. There some data on other gases: O_2, CO, NO, HCl, Cl_2, H_2O, N_2O, NH_3, and CH_4. These data for the processes occurring via the Langmuir–Hinshelwood mechanism (a reaction in the adsorbed layer) are collected in Table 1. It contains the results for the simplest cases when desorption flows have the maximal intensity in the direction of the normal to the surface (normal distributions). These flows are described by Eqs. (3) or (7), depending only on the polar angle φ between the normal to the surface and the velocity vector of a desorbing molecule.

2.2. The Role of the Precursor State

As can be seen from Table 1, Eq. (7) frequently describes the observed SDDFs more accurately than Eq. (3). This can be explained by the fact that adsorption–desorption processes often occur via the precursor state [77], which is analogous to physical adsorption. If some of the desorbing molecules remain in the precursor state for a time sufficient for relaxation, they leave the surface with thermal velocities and their SDDF is described by Eq. (2), that is, by the Knudsen law.

It has been shown in numerous experiments that, for SDDFs describable by Eq. (7), fast molecules are characterized by the sharply peaked distribution, whereas thermolyzed molecules are characterized by the Knudsen distribution.

Thus, SDDF makes it possible to estimate the contribution of the precursor pathway to the desorption rate.

The value of a in Eq. (7) determines the contribution of the molecules desorbed through the precursor state only for the molecules that leave the surface along the normal. In this case we are interested in their fraction b in the overall flow F from the surface. For an isotropic surface, F can be described by the integral [46] in spherical polar coordinates:

$$F = 2\pi \int_0^{\pi/2} I \sin\varphi \, d\varphi, \qquad (8)$$

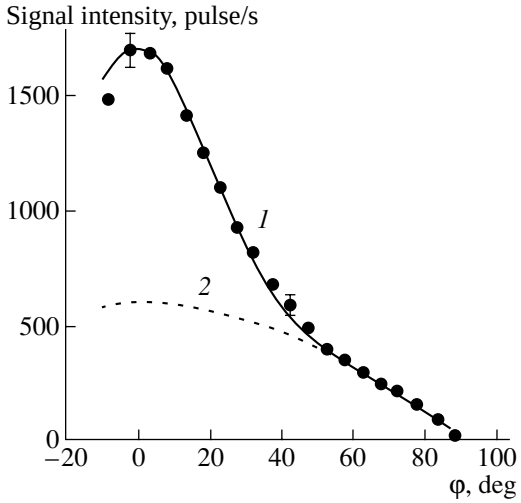

Fig. 5. SDDF described by the Comsa model for CO_2 molecules formed by CO oxidation on Pt(111) at 550 K [26]: (*1*) approximation of experimental data by Eq. (7) with $n = 8.3$ and $a = 0.35$ and (*2*) contribution of the Knudsen (cosine) distribution (Eq. (2)).

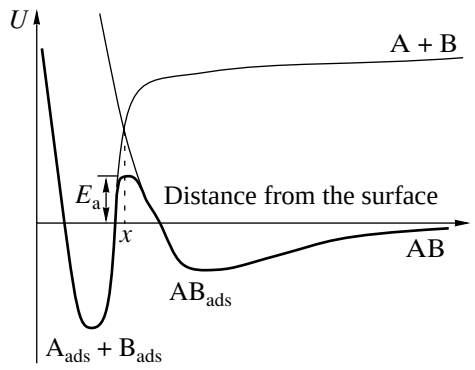

Fig. 6. Potential of the interaction *U* of the AB molecule with the surface as a combination of two Lennard–Jones curves corresponding to molecular (AB) and dissociative (A + B) adsorption.

where the polar axis coincides with the surface normal. After substituting the expression of *I* from (7) into Eq. (8), we obtain

$$F = 2\pi I_0 \int_0^{\pi/2} [(1-a)\cos^n\varphi + a\cos\varphi]\sin\varphi d\varphi. \quad (9)$$

In this approximation, integral (9) can be taken in the explicit form

$$F = 2\pi I_0[2 + a(n-1)]/(n+1), \quad (10)$$

and the value of *b* is determined by the simple formula

$$b = \left(2\pi a I_0 \int_0^{2/\pi} \cos\varphi\sin\varphi d\varphi\right)/F = a(n+1)/[2 + a(n-1)]. \quad (11)$$

The values of *b* calculated by formula (11) are shown in Fig. 7 in the form of dependences of *b* on *a* for several values of *n*. It is seen that *b* is much higher than *a* especially at high values of *n*. For instance, at $n = 40$–80 and $a = 5\%$, which is almost impossible to determine in SDDF measurements, *b* is 50–70%!

2.3. The Surface Relief, Anisotropy, and Directed Desorption

Models considered in the previous sections and the corresponding equations referred to ideal smooth flat surfaces. If a surface is not of this sort (e.g., a polycrystalline surface), SDDF becomes broader. The approximation of such distributions by Eqs. (1) or (3) gives effective values of parameters $n(n_{eff})$ and $\varepsilon(\varepsilon_{eff})$, which are underestimated compared to the true values n_{true} and ε_{true} corresponding to the ideal smooth surfaces.

Kislyuk and Bakuleva [78] proposed a model for the description of SDDF for the case of rough surfaces. This model considered a quasiflat surface consisting of flat elements each characterized by its polar angle α, which characterizes the deviation of the local normal to the average normal to the surface, and by angle ρ between the chosen direction on the surface and the projection of the local normal to the surface. For an element of the surface, SDDF was described by Eq. (3) applied to the local normal. In this case, SDDF can be described in the following form:

$$I/I_0 = \frac{\int_0^{2\pi} d\rho \int_0^{\pi/2} f(\alpha,\rho)[\sin\varphi\sin\alpha\cos(\rho-\rho_0) + \cos\varphi\cos\alpha]^n d\alpha}{\int_0^{2\pi} d\rho \int_0^{\pi/2} f(\alpha,\rho)\cos^n\alpha d\alpha}, \quad (12)$$

where $f(\alpha, \rho)$ is the distribution function of elementary areas, and ρ_0 is the azimuthal angle of observation. For an isotropic surface, this distribution function was independent of ρ (in [78], ρ was used instead of β).

To study the effect of isotropic surface roughness on SDDF, we considered substantially different distribution functions $f(\alpha)$ and calculated the dependences of n_{eff} on n_{true} at the roughness coefficient γ ranging from

Table 1. Parameters of spatial distributions of molecules desorbing along the normal to the surface and translational temperatures (T_{tr})

System	Methods and processes	T_{surf}, K	T_{tr}, K	Equation	n	Ref.
D_2/Ag(111)	TPD	190	–	(7)	8	[27]
	$2D_{ads} \longrightarrow D_2$					
H_2/Cu(100)	DMM	1100	–	(3)	5	[11]
H_2/Cu(110)	$2H_{ads} \longrightarrow H_2$	1100	–	(3)	2.5	
H_2/Cu(111)		1100	–	(3)	6	
HD/Cu(100)	MB, SSCR	850	–	(3)	5	[12]
HD/Cu(110)	$H_2 + D_2 \longrightarrow 2HD$	800–1100	–	(3)	2.5	
HD/Cu(310)		850	–	(3)	5.5	
H_2, D_2/Cu(111), Cu(100)	DMM, VM					[28]
	$2H_{ads} \longrightarrow H_2$	1000	4000	(3)	8 ± 1	
	$2D_{ads} \longrightarrow D_2$	1000	4000	(3)	8 ± 1	
H_2, HD, D_2/Cu(111)	MB, DMM					[29]
	$2H_{ads} \longrightarrow H_2$	370	–	(3)	14	
	$2D_{ads} \longrightarrow D_2$	600	–	(3)	12	
	$H_{ads} + D_{ads} \longrightarrow HD$	800	–	(3)	10	
H_2/Fe(poly)	DMM	900	–	(3)	6.5 ± 1.0	[1]
	$2H_{ads} \longrightarrow H_2$					
H_2/Fe(100)	TPD	420	–	(7)	2.0 ± 0.1	[31]
	$2H_{ads} \longrightarrow H_2$					
H_2/Ir(poly)	TPD	460	–	(3)	1.1 ± 0.2	[32]
	$2H_{ads} \longrightarrow H_2$					
H_2/Ni(poly)	DMM	900	–	(3)	10 ± 2	[1]
	$2H_{ads} \longrightarrow H_2$					
D_2/Ni(111)	DMM, VM	1143	1840	(3)	4 ± 1	[4]
	$2H_{ads} \longrightarrow H_2$					
HD/Ni(111)	MB, SSCR	700	–	(3)	2.5–4	[33]
	$H_2 + D_2 \longrightarrow 2HD$					
H_2/Ni(111)	DMM	925–1225	–	(2)	1	[34]
H_2/Ni(110)	$2H_{ads} \longrightarrow H_2$	925–1225	–	(2)	1	
H_2/Ni(111)	TPD	320–430	–	(3)	4.5	[35]
H_2/Ni(110)	$2H_{ads} \longrightarrow H_2$	320–430	–	(3)	1.2	
H_2/Ni(111)	TPD	290	–	(2)	1	[36]
	$2H_{ads} \longrightarrow H_2$	370	–	(3)	4.5	
D_2, HD/Ni(110)	TPD, SSCR, VM					[37]
	$2H_{ads} \longrightarrow D_2$	350	500	(3)	3.0 ± 0.5	
	$H_2 + D_2 \longrightarrow 2HD$	500	750	(3)	3.0 ± 0.5	
H_2/Pd(poly)	DMM	900	–	(3)	4.0 ± 0.5	[1]
	$2H_{ads} \longrightarrow H_2$					
D_2/Pd(100)	DMM, VM	360	360	(2)	1	[38]
	$2D_{ads} \longrightarrow D_2$	360	1030*	(7)	10	
HD/Pt(111)	MB, SSCR, VM					[39]
	$H_2 + D_2 \longrightarrow 2HD$	570–1200	$2T_{surf}$	(7)	5	
HD/Pt(557)	MB, SSCR, VM					[40]
	$H_2 + D_2 \longrightarrow 2HD$	500–1170	$0.75T_{surf}$	(3)	2	

Table 1. (Contd.)

System	Methods and processes	T_{surf}, K	T_{tr}, K	Equation	n	Ref.
D_2/Si(100)	TPD	825	–	(3)	4–5	[41, 42]
	$2D_{ads} \longrightarrow D_2$					
D_2/Si(100)	TPD	650	–	(3)	5 ± 1	[43]
	$2D_{ads} \longrightarrow D_2$					
N_2/Ag(111)	TPD	406, 443	–	(3)	75 ± 5	[44]
	$2N_{ads} \longrightarrow N_2$					
N_2/Ag(110)	TPD	520	–	(7)	12 ± 1	[45]
	$2N_{ads} \longrightarrow N_2$					
N_2/Cu(111)	MB, TPD, VM	700	21000	(3)	28 ± 1	[10]
	$2N_{ads} \longrightarrow N_2$					
N_2/Fe(poly)	TPR	770	–	(7)	4.4 ± 1.6	[46]
	$2NO_{ads} \longrightarrow N_2 + O_2$					
N_2/Ir(poly)	TPR, VM	500	3000 ± 1000	(3)	12 ± 2*	[47]
	$2NO_{ads} \longrightarrow N_2 + O_2$					
N_2/Mo(poly)	TPD	1200	–	(7)	4.4 ± 1.6	[46]
	$2N_{ads} \longrightarrow N_2$					
N_2/Pt(poly)	TPR	500	–	(3)	10 ± 3*	[48]
	$2NO_{ads} \longrightarrow N_2 + O_2$					
N_2/Rh(111)	SSCR, VM	620	2280	–	–	[9]
	$NO + H_2 \longrightarrow 1/2N_2 + H_2O$	800	2700	(7)	25 ± 5	
		1000	3200	–	–	
N_2/Ru(001)	SSCR, VM	900	3150	(3)	7 ± 3	[49]
	$2NH_3 \longrightarrow N_2 + 3H_2$					
N_2/W(110)	TPD	1600	–	(3)	3.0 ± 0.5	[50]
N_2/W(310)	$2N_{ads} \longrightarrow N_2$	1400	–	(3)	1.0 ± 0.2	
O_2/Ag(110)	TPD	600	–	(3)	4	[45]
	$2O_{ads} \longrightarrow O_2$					
O_2/Ir(poly)	TPR	1100	–	(7)	3.5 ± 1.5	[46]
	$2NO_{ads} \longrightarrow N_2 + O_2$					
O_2/Pt(111)	TPD	600–1000	–	(3)	2.0 ± 0.5	[51]
	$2O_{ads} \longrightarrow O_2$					
O_2/Pt(poly)	TPR	1100	–	(3)	1.6 ± 0.2	[52]
	$2NO_{ads} \longrightarrow N_2 + O_2$					
O_2/Pt(113)	TPD					[53]
	$2O_{ads} \longrightarrow O_2$	700–900	–	(2)	1	
	$O_{2,\,ads} \longrightarrow O_2$	140–200	–	(2)	1	
CO/Ir(poly)	TPD, VM	530	505 ± 170	(3)	1.1 ± 0.2	[47]
	$CO_{ads} \longrightarrow CO$	620	820 ± 180	(3)	1.1 ± 0.2	
CO/Ir(poly)	TPR	570–820	–	(3)	2–3	[54]
	$C_{ads} + O_{ads} \longrightarrow CO$					
CO/Ni(111), (110)	TPD	–	–	(2)	1	[13]
	$CO_{ads} \longrightarrow CO$	–	–	(2)	1	
CO/Pt(111)	TPR					[54]
	$C_{ads} + O_{ads} \longrightarrow CO$	800–100	–	(3)	2	
CO/Pt(poly)	TPD	600	–	(3)	1.1 ± 0.2	[52]
	$CO_{ads} \longrightarrow CO$					

Table 1. (Contd.)

System	Methods and processes	T_{surf}, K	T_{tr}, K	Equation	n	Ref.
CO/Pt(poly)	SSCR					[55]
	$C_{ads} + O_{ads} \longrightarrow CO$	1190	–	(3)	2.7 ± 1.0	
	$C_{ads} + 1/2O_2 \longrightarrow CO$	1190	–	(3)	4.5 ± 1.5	
CO/Rh(111)	TPR	520–700	–	(3)	1.5	[54]
	$C_{ads} + O_{ads} \longrightarrow CO$					
CO/W(100)	TPD/TPR					[56]
	$CO_{ads} \longrightarrow CO$	320–360	–	(3)	1.0 ± 0.5	
	$C_{ads} + O_{ads} \longrightarrow CO$	700–940	–	(3)	4 ± 1	
		940–1100	–	(3)	3 ± 1	
		1100–1500	–	(3)	1.5 ± 0.5	
CO/W(poly)	TPR	900	–	(3)	3.5 ± 0.4	[57]
	$C_{ads} + O_{ads} \longrightarrow CO$					
NO/Ir(poly)	TPD	350	500 ± 300	(3)	1.2 ± 0.3	[47]
	$NO_{ads} \longrightarrow NO$					
NO/Pt(111)	SSCR	550–1100	–	(3)	1.5	[58]
	$NH_3 + O_2 \longrightarrow NO + H_2O$					
NO/Rh(111)	SSCR, VM	600	1450	(7)	2.8	[59]
	$NO_2 + H_2 \longrightarrow NO + H_2O$	800	1860	(3)	1.5	
		1000	2030	(3)	1.2	
HCl/Au(111)	MB, SSCR, VM	300	200–300	(3)	1.4 ± 0.3	[6]
	$H_{ads} + Cl_{ads} \longrightarrow HCl$					
CO_2/Pd(111)	MB, SSCR	570	–	(2)	1	[60]
	$CO + 1/2O_2 \longrightarrow CO_2$					
CO_2/Pd(111)	SSCR, VM	500	1750 ± 100	(7)	5 ± 1	[61]
	$CO + 1/2O_2 \longrightarrow CO_2$					
CO_2/Pd(111)	TPR	230	–	(3)	20–40	[62, 63]
	$CO_{ads} + O_{ads} \longrightarrow CO_2$	270	–	(3)	12–25	
		400–500	–	(3)	4–8	
CO_2/Pd(100)	TPR	120	–	(3)	15 ± 2	[64]
	$CO_{ads} + O_{ads} \longrightarrow CO_2$	240	–	(3)	13 ± 3	
		290	–	(3)	11 ± 3	
		350	–	(3)	8 ± 1	
		400	–	(3)	7 ± 1	
CO_2/Pd(100)	SSCR, VM	460	1300–1600	(7)	11 ± 2	[65]
	$CO + 1/2O_2 \longrightarrow CO_2$	550	1500–1700	(7)	11 ± 2	
		700	1600–2100	(7)	11 ± 2	
CO_2/Pt(111)	MB, SSCR	450–950	–	(3)	6	[66]
	$CO + 1/2O_2 \longrightarrow CO_2$					
CO_2/Pt(111)	MB, SSCR	90	–	(3)	12 ± 1	[67]
	$CO + O \longrightarrow CO_2$					
CO_2/Pt(111)	TPR	160	–	(3)	13–19	[68]
	$CO_{ads} + O_{ads} \longrightarrow CO_2$	260	–	(3)	8–10	
CO_2/Pt(111)	MB, SSCR	470, 580	–	(7)	7 ± 1	[69]
	$CO + 1/2O_2 \longrightarrow CO_2$					

Table 1. (Contd.)

System	Methods and processes	T_{surf}, K	T_{tr}, K	Equation	n	Ref.
CO_2/Pt(111)	SSCR, VM	145	2030	(3)	8	[5]
	$CO + 1/2O_2 \longrightarrow CO_2$	210	1290	(3)	>10	
		250	1500	(3)	>10	
		330	1910	(7)	9	
CO_2/Pt(111)	MB, SSCR	550	–	(7)	7.5	[26, 70]
	VM	550–800	$4T_{surf}$	(7)	8–9	
	$CO + 1/2O_2 \longrightarrow CO_2$					
CO_2/Rh(poly)	TPR	280	–	(7)	8	[71]
	$CO_{ads} + O_{ads} \longrightarrow CO_2$	410	–	(7)	5	
	$CO_{2,\,ads} \longrightarrow CO_2$	120	–	(2)	1	
CO_2/Rh(111)	TPR	400	–	(7)	15 ± 3	[20]
	$CO_{ads} + O_{ads} \longrightarrow CO_2$	500	–	(3)	4 ± 1	
CO_2/Rh(111)	MB, SSCR	500	1170	(7)	9.4	[72, 73]
	VM	550	1370	–	–	
	$CO + 1/2O_2 \longrightarrow CO_2$	600	1650	–	–	
CO_2/Rh(110)	TPR	200	–	(3)	12 ± 2	[74]
	$CO_{ads} + O_{ads} \longrightarrow CO_2$	300	–	(3)	5 ± 1	
		400	–	(3)	3.0 ± 0.5	
		450	–	(3)	2.0 ± 0.5	
CH_4/Cu(poly)	TPR, VM	520	6000 ± 1000	(3)	>60*	[75]
	$CH_{3,\,ads} + H_{ads} \longrightarrow CH_4$					
CH_4/Mo(poly)	TPR	870	–	(3)	50 ± 20*	[46]
	$CH_{3,\,ads} + H_{ads} \longrightarrow CH_4$					
CH_4/Pt(111)	TPR	240	–	(3)	37	[76]
	$CH_{3,\,ads} + H_{ads} \longrightarrow CH_4$					

Note: TPR—temperature-programmed reaction; TPD—temperature-programmed desorption; DMM—diffusion through a metallic membrane; MB—molecular beams; SSCR—steady-state catalytic reaction; VM—velocity measurements.
* The values of n calculated taking into account the surface roughness according to the plot on Fig. 8 for $\gamma = 1.1$.

1.01–1.20 (Fig. 8). Analytical expressions for the value γ in Table 2 were determined from the equation [78]

$$\gamma = \left(\int_0^{\pi/2} f(\alpha)\,d\alpha\right) \Big/ \left(\int_0^{\pi/2} f(\alpha)\cos\alpha\,d\alpha\right) \qquad (13)$$

by substituting various distribution functions into it.

As can be seen from Fig. 8, the dependences of n_{eff} on n_{true} are largely determined by the value of γ and change insignificantly with a change in the form of function $f(\alpha)$. Thus, a correct study of SDDF is possible on rough surfaces, although the roughness coefficient should be rather low (≤1.10), which is characteristic of annealed surfaces.

Kislyuk *et al*. [57] experimentally studied the effect of surface relief on SDDF for the recombinative desorption of CO from the polycrystalline tungsten surface characterized by scanning tunneling microscopy (STM). The results agreed very well with the above model of the rough surface.

Anisotropic SDDFs were discovered by Matsushima for CO oxidation on the stepped Pd(110) surface [14]. In that case, the maximal intensity of the desorption flow was observed along the surface normal. However, in contrast to more complex cases, SDDF also depended on the azimuthal angle ψ. The distributions were sharply peaked in the direction [001] and rather broad in the direction $[1\bar{1}0]$.

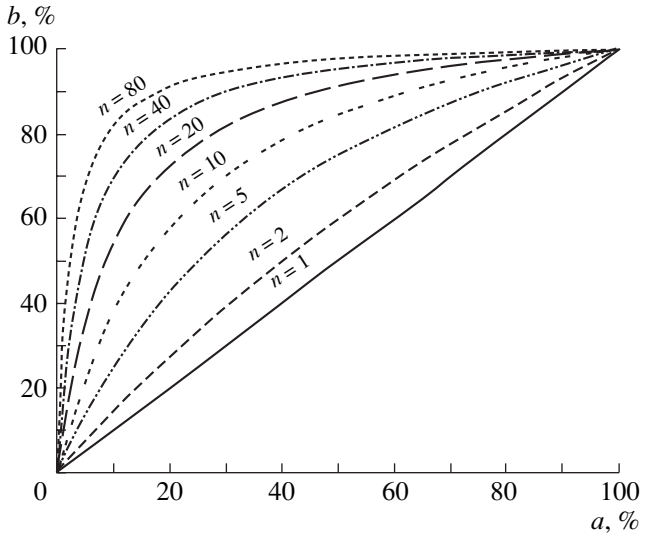

Fig. 7. Dependence of b on a calculated by formula (11) for various values of n.

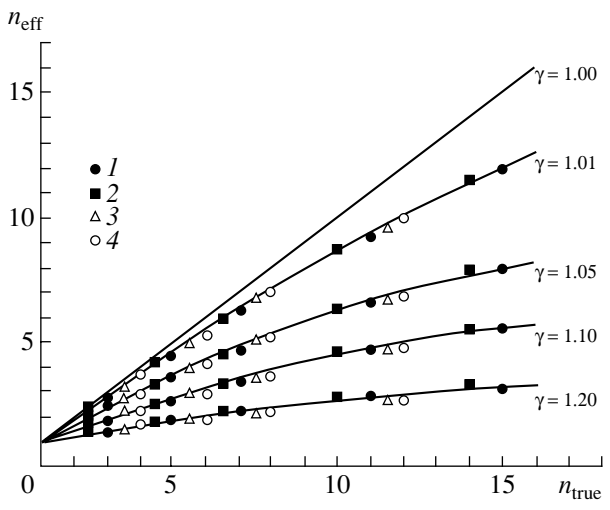

Fig. 8. Dependence of n_{eff} on n_{true} at different values of γ [78]. Models are numbered similarly to those in Table 2.

In 1990, Matsushima discovered the collimated desorption of CO_2 molecules in CO oxidation on the reconstructed Pt(110)(1×2) surface [15]. The maximums of SDDF were observed at certain angles to the surface normal.

More recently, several researchers observed different cases of anisotropic and collimated desorption [57, 79–84].

To describe SDDF in cases of anisotropic and collimated desorption, the following empirical equations were proposed [85, 86]:

$$I/I_0 = (\cos\varphi)^{n(\cos\psi)^2 + m(\sin\psi)^2}, \quad (14)$$

$$I/I_0 = (\cos(\varphi - \varphi_0))^{n(\cos\psi)^2 + m(\sin\psi)^2}, \quad (15)$$

where φ is the polar angle, ψ is the azimuthal angle with respect to the step direction, φ_0 is the collimation angle (a polar angle between the normal and the direction corresponding to the maximal SDDF intensity), and n and m are the exponents determining the sharpness of SDDF in the planes that are parallel and perpendicular to the direction of steps.

Figure 9 shows anisotropic and collimated SDDF measured by Matsushima and coworkers [14, 15, 80]. Note that both wings of the collimated distribution (Fig. 9b) are also anisotropic. They are approximated by Eq. (15) with $n = 12$ and $m = 6$ in the directions [001] and $[1\bar{1}0]$, respectively.

Table 3 collects data for the processes occurring on stepped surfaces via the Langmuir–Hinshelwood

Table 2. Distribution functions of elementary surface areas and expressions for the roughness coefficients

Model	Distribution function*	Roughness coefficient
1	$f(\alpha) = \begin{cases} A, 0 \le \alpha \le \alpha_0 \\ 0, \alpha > \alpha_0 \end{cases}$	$\gamma = \dfrac{\alpha_0}{\sin\alpha_0}$
2	$f(\alpha) = \begin{cases} B(\alpha_0 - \alpha), 0 \le \alpha \le \alpha_0 \\ 0, \alpha > \alpha_0 \end{cases}$	$\gamma = \dfrac{\alpha_0^2}{2(1 - \cos\alpha_0)}$
3	$f(\alpha) = \begin{cases} C\alpha, 0 \le \alpha \le \alpha_0 \\ 0, \alpha > \alpha_0 \end{cases}$	$\gamma = \dfrac{\alpha_0^2}{2(\alpha_0\sin\alpha_0 + \cos\alpha_0 - 1)}$
4	$f(\alpha) = \begin{cases} D\alpha(\alpha_0 - \alpha), 0 \le \alpha \le \alpha_0 \\ 0, \alpha > \alpha_0 \end{cases}$	$\gamma = \dfrac{\alpha_0^2}{6(2\sin\alpha_0 + \alpha_0\cos\alpha_0 - \alpha_0)}$

* A, B, C, and D are the normalization constants.

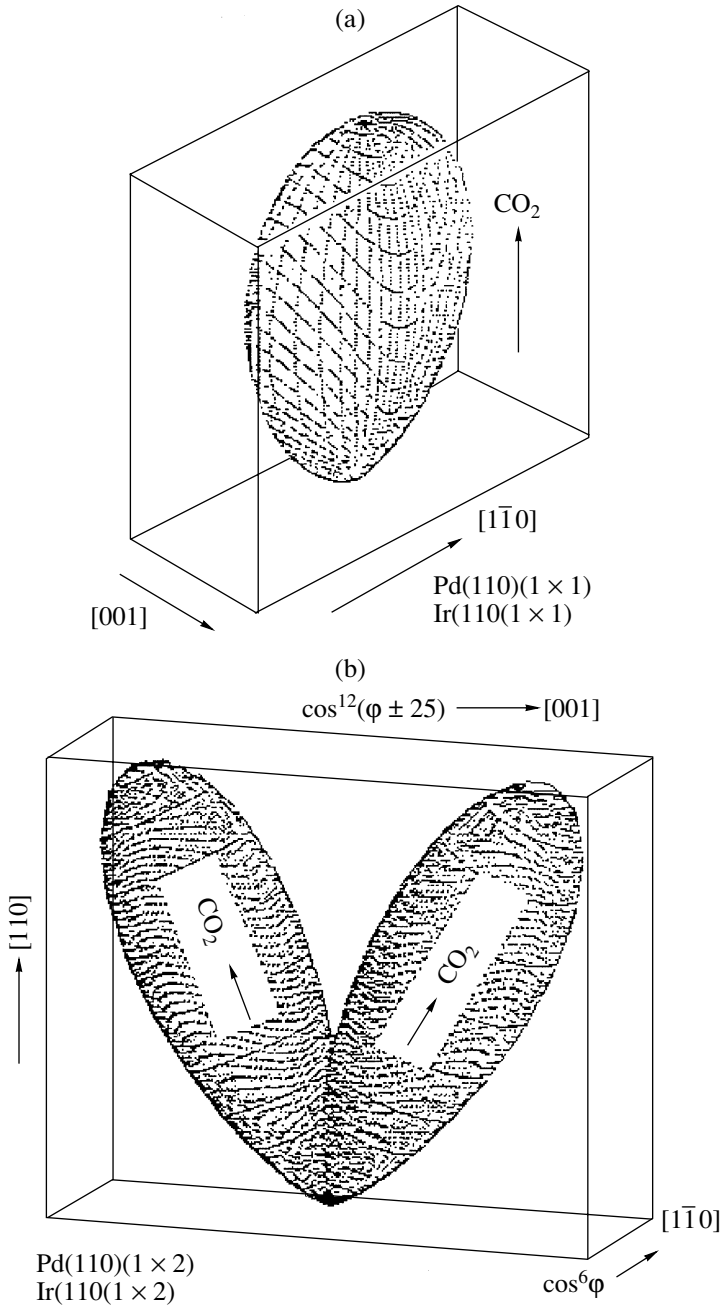

Fig. 9. (a) Anisotropic and (b) collimated distributions in CO_2 desorption in CO oxidation on the (110)(1 × 1) and (110)(1 × 2) surfaces of platinum-group metals [14, 15, 80].

mechanism where anisotropic and collimated distributions were observed.

2.4. Translational Energy of Desorbing Molecules

The measurements of velocity distributions of desorbing molecules provide information on the process dynamics. Although SDDF is largely determined by the ratio of the normal component of the velocity to the tangential component, one should avoid estimating E_a from sole spatial distributions, which are sensitive to the state of the surface. SDDF can broaden because of surface roughness as a result of argon ion bombardment, oxidation reactions, surface reconstruction, and other factors.

Some general features of the velocity distributions of desorbing molecules have been determined experimentally. The translational temperature T_{tr} of molecules is usually higher than the surface temperature T_{surf}. The apparent velocity distributions of molecules can be

Table 3. Parameters of anisotropic and collimated spatial distributions of molecules desorbing from stepped surfaces and their translational temperatures

System	Methods and processes	Measurement plane	T_{surf}, K	T_{tr}, K	n	φ_0, deg	Ref.
N_2/Pd(110)	TPR						[81, 87]
	$NO_{ads} \longrightarrow 1/2N_2 + O_{ads}$	⊥	490	–	46	±38	
		∥	490	–	14	±38	
		⊥	490	–	4.2	0	
		∥	490	–	4.2	0	
	$2N_{ads} \longrightarrow N_2$	⊥	460	–	6–7	0	
		⊥	540	–	4 ± 1	0	
	$^{15}N_{ads} + {}^{14}NO_{ads} \longrightarrow N_2 + O_{ads}$	⊥	490	–	20 ± 5	±38	
	SSCR						
	$2NO + 2H_2 \longrightarrow N_2 + 2H_2O$	⊥	600	–	1	0	
N_2/Pd(110)	TPR, VM						[88]
	$NO_{ads} \longrightarrow 1/2N_2 + O_{ads}$	⊥	490	2700	28	±41	
		⊥	490	1300	28	±41	
		⊥	490	–	5	0	
	$N_2O_{ads} \longrightarrow N_2 + O_{ads}$	⊥	140	2700	60	±43	
		⊥	140	1300	60	±43	
		⊥	140	–	3	0	
		⊥	152	1930	50	±43	[89]
		⊥	152	580	–	±43	
	SSCR, VM	⊥	350–750	2660	28	±41	[90]
	$6NO + 4CO \longrightarrow N_2 + 2N_2O + 4CO_2$	⊥	350–750	1300	28	±41	
		⊥	350–750	–	5	0	
N_2/Pd(210)	TPR						[91]
	$N_{ads} + NO_{ads} \longrightarrow N_2 + O_{ads}$	⊥	470–510	–	20	–25…–30	
		∥	510	–	1	0	
	$2N_{ads} \longrightarrow N_2$	⊥	470	–	4	0	
N_2/Rh(533)	TPR						[82]
	$NO_{ads} \longrightarrow 1/2N_2 + O_{ads}$	⊥	450	–	4	–15	
		⊥	600	–	4	–15	
CO/Pt(110)	MB						[84]
(1 × 2)	$C_{ads} + 1/2O_2 \longrightarrow CO$	⊥	650	–	50 ± 5	±32	
NO/Ag(110)	TPR	⊥	520	–	5 ± 1	0	[45]
	$N_{ads} + O_{ads} \longrightarrow NO$	∥	520	–	40–50	0	
		∥	520	–	40–50	±17	
CO_2/Ir(110)	TPR						[79, 80]
(1 × 1)	$C_{ads} + 1/2O_2 \longrightarrow CO$	∥	380	–	10	0	
		⊥	380	–	3.5	0	
CO_2/Ir(110)		∥	380	–	7	0	
(1 × 2)		⊥	380	–	18	±26	
CO_2/Pd(110)	TPR, VM	⊥	460	2400	10 ± 2	0	[92–94]
	$CO_{ads} + O_{ads} \longrightarrow CO_2$	⊥	420–460	1350	10 ± 2	0	
		∥	420–460	1350	3.0 ± 0.5	0	
		⊥	350	1520	10 ± 3	0	
		∥	350	1520	4.0 ± 0.5	0	
		⊥	290	1750	15 ± 3	0	
		∥	290	1750	8 ± 2	0	
		⊥	230	2000	20 ± 4	0	
		∥	230	2000	15 ± 2	0	
		⊥	170	2240	25 ± 5	0	
		∥	170	2240	20 ± 5	0	

Table 3. (Contd.)

System	Methods and processes	Measurement plane	T_{surf}, K	T_{tr}, K	n	φ_0, deg	Ref.
CO_2/Pd(110)	SSCR, VM						[86, 90, 95–97]
	$CO + 1/2O_2 \longrightarrow CO_2$	⊥	450–460	1300–2400	10–20	0	
	$4CO + 6NO \longrightarrow 4CO_2 + N_2 + 2N_2O$	⊥	540	–	15 ± 3	0	
		‖	–	1330	3	0	
CO_2/Pd(110)	SSCR						[87]
	$4CO + 6NO \longrightarrow 4CO_2 + N_2 + 2N_2O$	⊥	490	–	9	0	
		⊥	600	–	4	0	
CO_2/Pt(110)	TPR, VM	⊥	310	1450	12 ± 3	±25	[94, 98]
	$CO_{ads} + O_{ads} \longrightarrow CO_2$	⊥	410	1450	12 ± 2	±23	
	SSCR, VM	⊥	500–550	1700 ± 100	6–9	±25	
	$CO + 1/2O_2 \longrightarrow CO_2$	⊥	–	1500	6–9	0	
CO_2/Pt(112)	TPR, VM	⊥	400	1210	8	–25	[99]
	$CO_{ads} + O_{ads} \longrightarrow CO_2$	⊥	400	1330	12	10	
		⊥	300	1240	8	–25	
		⊥	300	1240	12–14	8–13	
		⊥	230	1100–1500	8–17	16–2	
CO_2/Pt(113)	TPR, VM	⊥	235–400	1320	12–15	21–25	[83, 85, 100–103]
	$CO_{ads} + O_{ads} \longrightarrow CO_2$	⊥	235–400	1150	9–13	–15…–17	
		‖	360–370	–	6–7	0	
		‖	280–300	–	7–10	0	
	SSCR, VM	⊥	555	2100	7	–20	
	$CO + 1/2O_2 \longrightarrow CO_2$	⊥	555	1650	7	22	
CO_2/Pt(557)	TPR						[104, 105]
	$CO_{ads} + O_{ads} \longrightarrow CO_2$	⊥	300–450	–	14	3	
	$CO_{ads} + 1/2O_{2,\,ads} \longrightarrow CO_2$	⊥	160	–	12	–7	
	SSCR, VM				–	–	
	$CO + 1/2O_2 \longrightarrow CO_2$	–	500–780	1200–2300			

Note: SDDFs are approximated by the equation $I/I_0 = \cos^n(\varphi - \varphi_0)$, where φ_0 is the collimation angle relative to the global surface normal and signs ⊥ and ‖ refer to the planes in which SDDFs were measured (normal and parallel to the steps). Abbreviations are the same as in Table 1.

divided into two components: the Maxwell distribution corresponding to the surface temperature,

$$f_1(r) = r^3 \exp(-Mr^2/2kT_{surf}), \quad (16)$$

and the modified Maxwell distribution,

$$f_2(r) = r^3 \exp[-(r - r_0)^2/g^2], \quad (17)$$

which describes fast molecules.

In Eqs. (16) and (17), $f_1(r)$ and $f_2(r)$ are the velocity (r) distribution functions, M is the molecular weight, k is the Boltzmann constant, r_0 is the velocity of the desorption flow, and g is the parameter determining the width of distribution.

The translational energy of fast molecules is determined by the formula

$$T_{tr} = \langle E \rangle / 2k, \quad (18)$$

where $\langle E \rangle$ is their average translational energy.

The van Willigen model postulates that the barrier is one-dimensional in the direction to the surface normal. It is assumed that only molecules possessing sufficient kinetic energy in the direction of normal are capable of

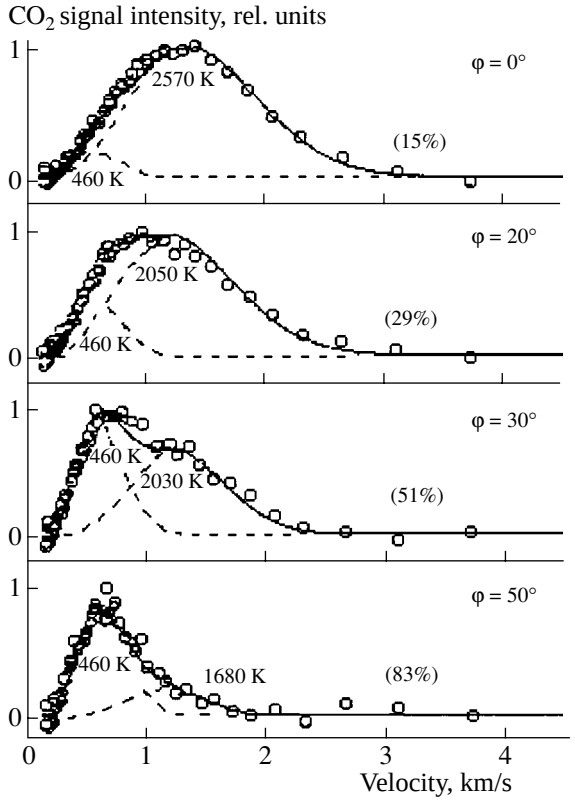

Fig. 10. Velocity distributions of CO_2 molecules at T_{surf} = 460 K and different desorption angles relative to the surface normal under conditions of the active regime (see section 3.2) of the steady-state reaction of CO oxidation on Pd(110) [86]. Dashed lines show the deconvolution of distribution into high-energy and low-energy components. The contributions of low-energy (thermal) molecules are shown in parentheses.

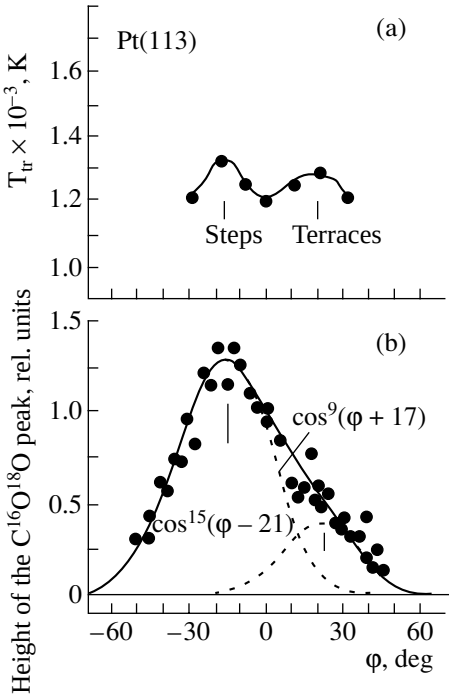

Fig. 11. Dependence of (a) the translational temperature and (b) the flow density of CO_2 on the desorption angles under conditions of $CO_{ads} + O_{ads} \longrightarrow CO_2$ TPR on Pt(113) at T_{surf} = 300 K registered in the direction perpendicular to steps [100]. Dashed lines shows the deconvolution of SDDF into two peaks. Surface coverages by molecular oxygen and carbon monoxide are $\theta_O = 0.3$ and $\theta_{CO} = 0.15$, respectively.

overcoming the barrier and adsorbing. According to the model and the principle of microscopic reversibility, the average translational energy $\langle E_\perp \rangle$ desorbing along the normal can be estimated as follows [72]:

$$\langle E_\perp \rangle \approx E_a + 2kT_{surf}. \quad (19)$$

Formulas (18) and (19) provide an estimate of the activation energy of adsorption E_a:

$$E_a \approx 2k(T_{tr\perp} - T_{surf}), \quad (20)$$

where $T_{tr\perp}$ is the translational temperature of molecules desorbing along the normal to the surface.

For the distributions of fast molecules concentrated along the surface normal, the maximal translational temperature is observed along the surface normal. For off-normal desorption, it is observed in the direction of the collimation angle φ_0. For slow molecules, $T_{tr} = T_{surf}$ independently of the velocity vector of the desorption molecules. Examples taken from [86, 100] are shown in Figs. 10 and 11.

Formulas (5) and (20) can be used to obtain the dependence of $T_{tr\perp}$ on n and T_{surf} for fast molecules desorbing along the surface normal [106]:

$$T_{tr\perp} = T_{surf}(n + 3)/4. \quad (21)$$

Although Eqs. (1), (3), (6), and (7) successfully describe the SDDFs observed, the one-dimensional model absolutely incorrectly predicts the dependence of the translational energy of desorbing molecules on the angle of their velocity vector. According to this model, only the normal component of the translational energy is important for overcoming the activation barrier. Therefore, the translational temperature of molecules desorbing at an angle φ to the normal should be

$$T_{tr}(\varphi) = T_{tr\perp}/\cos^2\varphi. \quad (22)$$

This means that the translational temperature should increase with an increase in φ. In fact, the reverse dependence is observed (Fig. 12) [73]. No example of increasing T_{tr} with an increase in φ was found in experiments.

The results of measurements of the velocities of fast desorbing molecules in the form of maximal values of T_{tr} along the normal or at a collimation angle are shown in Tables 1 and 3.

2.5. From the Two-Dimensional Model to Multidimensional Models

The discussion below mostly refers to the H_2/Cu system, which is a classical example of direct dissociative activated adsorption, which was studied both theoretically and experimentally in most detail [30].

As was shown in the preceding sections, the van Willigen one-dimensional model, which takes into account only the translational energy, has some limitations and does not provide a correct description of the velocities of desorbing molecules on the angle of their emission from the surface, nor does it correctly describe anisotropic and directed desorption. All these limitations are due to the assumptions that neglect the structure of the surface and internal degrees of freedom of desorbing molecules.

The role of vibrational degrees of freedom in direct dissociative activated adsorption can be estimated for the simplest case of a diatomic molecule with an axis parallel to the surface. The two dimensional potential of such a system is qualitatively shown in Fig. 13 [107], where one coordinate (*Z*) is the distance of a molecule from the surface, and the other is the distance (*Y*) between the atoms in a molecule.

At high values of *Z*, the potential energy surface is determined by the potential of interaction of atoms in the gaseous molecule. At high values of *Y*, it corresponds to the interaction of adsorbed atoms with the surface. The barrier is between two valleys. The adsorption–desorption dynamics is the most sensitive to the topography of this transient region, especially to the position of a saddle of the activation barrier marked with a cross.

If the saddle is at the entrance of the adsorption channel, then the initial translational energy is more efficient for dissociative chemisorption than the vibrational energy (see Figs. 13a and 13b). Considering the reverse trajectories according to the principle of microscopic reversibility, we obtain that energy released in the course of desorption mostly transforms into the translational energy of a desorbing molecule.

The opposite situation occurs when the saddle is at the exit of the channel. The initial vibrational excitation of a molecule is favorable for overcoming the barrier (Fig. 13c), and the translation energy is inefficient (Fig. 13d). In this case, according to the principle of microscopic reversibility, we obtain that most of the energy of desorbing molecules transforms into its vibrational excitation.

In 1985, Harris and Andersson [108] calculated the potential of interaction for the H_2/Cu system based on the full energy of the H_2Cu_2 cluster (Fig. 14). This potential includes two regions: *I* is the entrance channel that controls the trajectories of H_2 molecules approaching the surface and *II* is the exit channel that determines the state of adsorbed atoms H. The calculated height of the barrier is ~1 eV. This value is much higher than the 0.3–0.4 eV obtained in adsorption measurements carried out by Balooch *et al.* [12], but it is rather close to the results of desorption measurements (0.87 eV) carried out by Comsa and David [28].

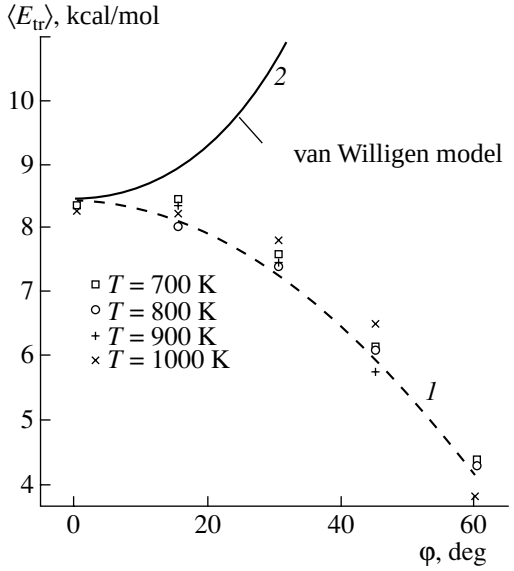

Fig. 12. Dependence of the average translational energy (⟨E_{tr}⟩) on the angle of CO_2 desorption formed under conditions of steady-state CO oxidation at different temperatures of the Rh(111) surface: (*1*) experiment [73] and (*2*) prediction by the van Willigen model (Eq. (22)).

The direct experimental method for the determination of E_a is possible when the supersonic molecular beam is directed to the surface at a certain angle and controlled by the kinetic energy of molecules. Note that supersonic molecular beams are characterized by very narrow, quasi-monoenergetic distributions of translational energy of molecules [19]. This method makes it possible to determine the probability of adsorption (the sticking coefficient *S*) depending on the energy of collision and the angle of an incident beam.

Results obtained by this method at different incident angles often depend on the normal translational energy $E_\perp$ associated with the momentum of molecules normal to the surface.

In 1989, two groups of researchers published data on the dissociative adsorption of H_2 on single crystal copper surfaces [109, 110]. They carried out measurements at different incident angles and varied the translational energy of the beam by changing the nozzle temperature. Figure 15 shows data obtained by Anger *et al.* [109]. Both groups observed a drastic increase in the sticking probability with an increase in the normal energy of beamed molecules in agreement with the predictions of the van Willigen model.

The main limitation of the model used in [109, 110] is that both the translational and vibrational energies of beamed molecules are proportional to the nozzle temperature. This effect prevented the researchers from

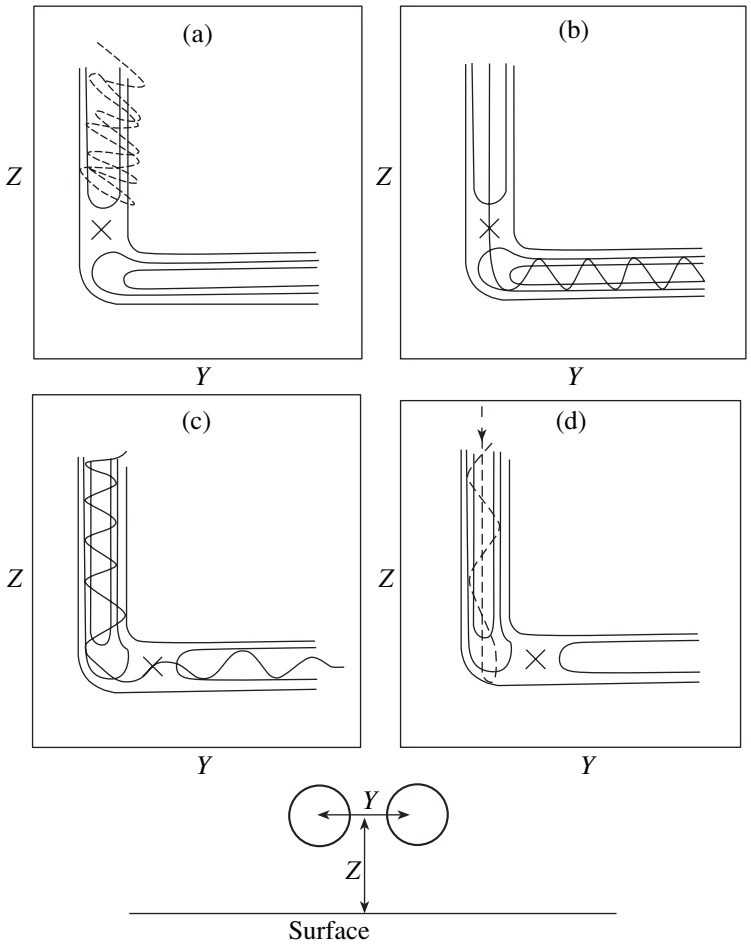

Fig. 13. Two-dimensional potential of the diatomic molecule with the surface at different positions of the saddle (a–d, see text) [107]. The cross marks the position of the activation barrier (saddle).

elucidating the role of vibrational excitation in adsorption.

The use of inert diluent in molecular beams made it possible to overcome this limitation. Rettner *et al*. [111] applied this method and obtained more complete data for the direct dissociative chemisorption of hydrogen on copper. Figure 16 shows the results of measurements of the initial sticking probability S_0 of deuterium on Cu(111) for molecular beams with translational energies of up to 0.85 eV, vibrational temperatures of up to 2100 K, and incident angles ranging from 0° to 60°.

These data obtained in a broad range of experimental conditions revealed the strong dependence of S_0 on both $E_\perp$ and the vibrational temperature T_{vib}. Therefore, these factors were both important for overcoming the activation barrier.

In a recent experimental study [112], Rettner *et al*. showed that the vibrational energy also plays a noticeable role in the dynamics of activated adsorption–desorption processes.

Attempts have been made to extend theoretical description to the multidimensional model. Calculations carried out in [113] showed that important dynamic effects are lost if one considers the fixed orientation of a molecule. Engdahl *et al*. [114] compared dynamic calculations of the H_2/Cu system in two and six dimensions and concluded that all six degrees of freedom of a hydrogen molecule should be considered when comparing the activities of different faces of copper single crystals.

3. REACTIONS OCCURRING VIA THE LANGMUIR–HINSHELWOOD MECHANISM

3.1. Desorption of Products along the Normal to the Surface

Hydrogen. The spatial distributions for the recombinative desorption of this gas on the surfaces of Fe, Ir, Ni, Pt, and Pd are rather broad (n = 1–5) and can be approximated by Eqs. (1) and (3). The values of E_a obtained for these metals using this approximation are rather low (<10 kJ/mol) [31, 32, 34, 36–38, 40, 115]

and correspond to the values calculated from kinetic data and the isosteric heats of adsorption [31, 115]. More sharply peaked SDDFs observed in earlier studies [1, 33–35, 39, 40] and, correspondingly, higher values of E_a were not confirmed. They can be explained by the effect of carbon, sulfur, and other admixtures [34, 38].

Sharply peaked SDDFs of hydrogen are observed on the surfaces of copper and silver [11, 12, 27–29]. The dissociative adsorption of hydrogen is practically not observed on these surfaces under ordinary conditions because of high activation energies [116].

The values of E_a (kJ/mol) for hydrogen on different faces of copper calculated on the basis of the van Willigen model with data presented in Table 1 are 19–29 [29] and 22 [11] for Cu(111), 7 [11, 12] for Cu(110), 28 [28] and 15–18 [11, 12] for Cu(100), and 15–19 for Cu(310). These data largely agree with those obtained from the sticking probability measurements of H_2 and D_2 using supersonic molecular beams [12], but they are much lower than the independent estimates E_a = 40–70 kJ/mol [27, 117–124].

The estimate of E_a according to the van Willigen model for D_2/Ag(111) is as low as 5 kJ/mol. Such a low activation barrier cannot explain the absence of the dissociative adsorption of hydrogen on silver. A relatively broad SDDF observed for this system points to the fact that the translational energy of desorbing molecules along the normal is lower than expected. In this system, some of the excess energy possibly transforms into the excitation of the internal degrees of freedom [27].

The results of hydrogen SDDF on Si(100) have recently been published [41–43].

Attempts have been made to detect the anisotropy of hydrogen SDDF on Cu(100), Cu(110) [11], and Ni(110) [35], but distributions registered at different angles were the same within the experimental error. Thus, no information was obtained on the surface structure from hydrogen SDDFs. This can be explained by the fact that a hydrogen molecule is formed rather far from the surface when two hydrogen atoms should move to the distance that is substantially longer than the bond distance in the H_2 molecule to be formed. As a result, hydrogen atoms "lose their memory" of the surface site structure. A similar lack of structural sensitivity is expected in the case of the recombinative desorption of nitrogen and oxygen.

It has been found recently [32] that the presence of coadsorbed CO significantly affect H_2 SDDF. In the absence of CO, the SDDF of hydrogen is described by the Knudsen law. In the case of desorption from the layer of coadsorbed CO and H_2, the SDDF of hydrogen concentrates along the normal to the sample surface. A model has been proposed to explain this "focusing" effect.

The measurement of velocities of hydrogen molecules desorbed from Cu(111), Cu(100) [28], Ni(111) [4], Ni(100) [37], and Pt(111) [39] revealed only the fast component, which is characterized by $T_{tr} = (1.5–4.0)T_{surf}$.

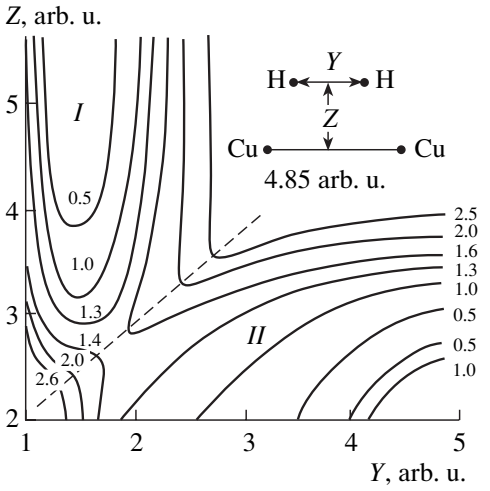

Fig. 14. The potential energy surface for the H_2/Cu system based on the calculated energy of the H_2Cu_2 cluster [108]. The values of energies (in eV) shown near the equipotential curves are calculated relative to the infinitely distant position of the H_2 from the surface ($Z = \infty$, Y = 1.4 arb. u.).

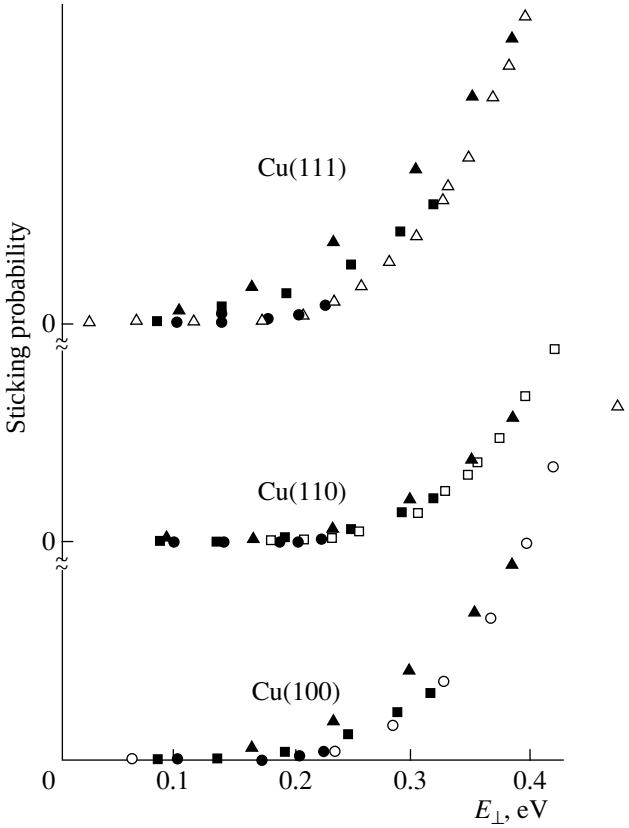

Fig. 15. Sticking probabilities of hydrogen (S) on three planes of a copper single crystal as functions of the normal beam energy ($E_\perp$) [109]. Different points show the results of measurement at different beam angles.

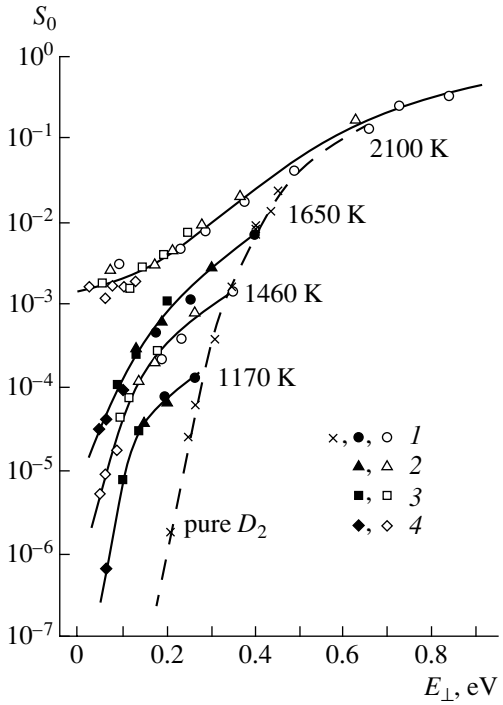

Fig. 16. The initial sticking probability S_0 of D_2 on Cu(111) for beams with a kinetic energy of up to 0.85 eV and a vibration temperature of up to 2100 K: (*1*) 0°, (*2*) 30°, (*3*) 45° and (*4*) 60° [111].

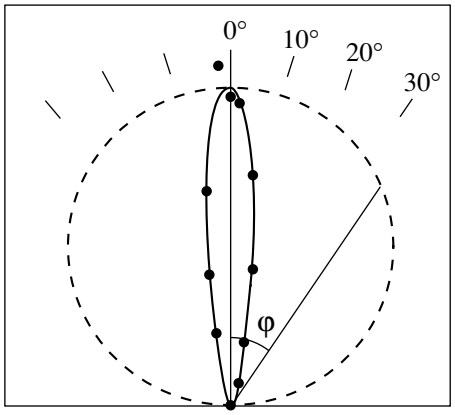

Fig. 17. Spatial distribution of desorbing N_2 molecules with an Ag(111) surface saturated with adsorbed nitrogen atoms [44]. The approximation is by Eq. (3) with $n = 75$; for comparison, cosine Knudsen distribution is shown.

On the clean Pd(100) surface, hydrogen desorption occurred with thermal velocities ($T_{tr} = T_{surf}$), but the fast component appeared in the case of sulfur admixtures [38].

In the rare cases when SDDF measurements were carried out simultaneously with the measurements of translational energies of desorbing hydrogen molecules, the values of E_a calculated by Eqs. (5) and (20) coincide. An exception is the early work by Lin and Somorjai [40] on the recombinative desorption of HD from Pt(557), where the translational temperature of molecules was lower than the surface temperature.

Nitrogen does not dissociate on most metals except for molybdenum [46], tungsten [50], and some others because of the high activation barrier [125]. For that reason, nitrogen desorption is studied on the surfaces with preadsorbed atomic nitrogen [10, 44] or in systems where surface reactions generate nitrogen: $2NO_{ads} \longrightarrow N_2 + O_2$ [46–48, 88, 90], $NO + H_2 \longrightarrow 1/2\ N_2 + H_2O$ [9], $2NH_3 \longrightarrow N_2 + 3H_2$ [49], and $2N_2O_{ads} \longrightarrow 2N_2 + O_2$ [88, 90].

Murphy *et al.* [10, 44] observed extremely sharply peaked SDDFs of nitrogen on copper and silver. Figure 17 shows the results obtained for N_2/Ag(111) [44]. In this case, data were described by Eq. (3) with $n = 75 \pm 5$. Very sharply peaked SDDFs were also found for N_2/Cu(111) with $n = 28 \pm 1$ [10] and N_2/Rh(111) with $n = 25 \pm 5$ [9]. Estimates made for these three systems using the van Willigen model and simple formula (5) gave the following values of E_a: 130 ± 20, 85 ± 15, and 90 ± 30 kJ/mol.

On the polycrystalline samples of Pt [48] and Ir [47], we obtained much lower values than for Rh: $n = 4 \pm 1$ and $n = 3.0 \pm 0.5$, respectively; $E_a = 7 \pm 1$ and $E_a = 4 \pm 1$ kJ/mol, respectively. This fact can be explained by the roughness of polycrystalline surfaces, which results in the broadening of SDDFs and a corresponding decrease in the value of n [78]. The values corrected considering surface roughness ($\gamma = 1.1$) are $n = 12 \pm 2$ (Ir) and $n = 10 \pm 3$ (Pt), and the corresponding values of activation energies are $E_a = 22 \pm 4$ and 18 ± 6 kJ/mol. It is noteworthy that T_{tr} of N_2 molecules desorbed from iridium was 3000 ± 1000 K [47], which corresponds to an E_a value of 40 ± 15 kJ/mol calculated using formula (20). This seems to be a better estimate of the activation barrier, because the direct measurements of velocities of desorbing molecules are almost independent of surface roughness. Moreover, the value of E_a explains the absence of dissociative adsorption on iridium.

Broad SDDFs of nitrogen were observed on iron and molybdenum [46], ruthenium [49], and tungsten [50]. This is not surprising because the values of E_a for nitrogen on these metals are rather low. For the N_2/W(310) system, Cosser *et al*. [50] observed Knudsen SDDF corresponding to nonactivated adsorption.

In addition to [47], the velocities of desorbing N_2 molecules were measured on Rh(111) [9], Cu(111) [10], and Ru(001) [49] (see Table 1). Only for ruthenium did the values of activation energies obtained from SDDF and the rate measurements agree with each other. For other metals, substantial differences are observed.

Oxygen readily dissociates on clean surfaces of most metals. The SDDF of recombinatively desorbed oxygen observed by the TPD/TPR methods on Pt, Pd, and Ir [47, 51–53] are broad (n = 1–2) and correspond

to a low value of the activation barrier $E_a < 4$ kJ/mol. The velocities of desorbing O_2 molecules for preadsorbed and preabsorbed oxygen on Rh(111) were measured in [126]. In both cases, the results coincided, pointing to the existence of a common activated complex in the desorption of surface and subsurface oxygen.

CO and NO. When these gases are adsorbed in molecular form, their SDDFs are accurately described by the Knudsen law [13, 35, 47, 48, 52, 56, 127, 128], which confirms the nonactivated chemisorption of these molecules. However, SDDF are more sharply peaked when these molecules are the products of heterogeneous processes: $C_{ads} + O_{ads} \longrightarrow CO$ [54–57], $C_{ads} + 1/2O_2 \longrightarrow CO$ [55], $NO_2 + H_2 \longrightarrow NO + H_2O$ [59], and $4NH_3 + 5O_2 \longrightarrow 4NO + 6H_2O$ [58]. For illustration, Fig. 18 shows SDDFs that are measured for CO molecules preadsorbed on the platinum surface and for the product of reactions $C_{ads} + O_{ads} \longrightarrow CO$ and $C_{ads} + 1/2O_2 \longrightarrow CO$ [55]. Gibson *et al*. [59] measured simultaneously SDDF and the velocities of NO molecules that were the product of the reaction $NO_2 + H_2 \longrightarrow NO + H_2O$ and found that $T_{tr} > T_{surf}$ and $n > 1$.

H_2O, N_2O, NH_3, HCl. There few papers devoted to the SDDF measurements of these molecules as products of the following processes: $H_2 + 1/2O_2 \longrightarrow H_2O$ on Pt(111) [129] and Rh(111) [130], $NO_{ads} + N_{ads} \longrightarrow N_2O$ on Pd(211) [91] and Pd(110) [131], $4CO + 6NO \longrightarrow 2N_2O + N_2 + 4CO_2$ on Pd(110) [90], $2NO + 5H_2 \longrightarrow 2H_2O + 2NH_3$ on Pd(110) [67], and $H_{ads} + Cl_{ads} \longrightarrow HCl$ on Au (111) [6].

SDDFs for these gases were very close to the Knudsen distribution, and the velocities of desorbing molecules (when they were measured [130]) were very close to thermal.

Methane. SDDF measurements of methane recombinative desorption ($CH_{3,\,ads} + H_{ads} \longrightarrow CH_4$) were carried out on Pt(111) [76], polycrystalline Mo [46], and polycrystalline Cu [75]. In all cases, sharply peaked SDDFs of methane were observed. We estimated E_a (kJ/mol) for these three systems using the van Willigen model: 35 ± 5(Pt), 50 ± 20 (Mo), and 32 ± 5 (Cu), which were rather close to the results of experiments on the dissociative adsorption of methane on metal surfaces from supersonic molecular beams [132–134].

The observed sharply peaked SDDFs of methane can be explained as follows. The adsorbed reactants, methyl and atomic hydrogen, are very close to the metal surface (at a distance of 1 Å). The diffusion of H_{ads} is much faster than $CH_{3,\,ads}$. Methane is probably formed on the sites occupied by $CH_{3,\,ads}$. The methane molecule is rather large (its Van-der-Waals radius is 2.6 Å). Therefore, the surface repulses it to produce a sharply peaked SDDF.

Only one study is known [75] where the average velocity of methane molecule desorption along the normal to the surface was measured. The translational temperature was 4000 ± 2000 K in that case. It corresponds to $E_a = 34 \pm 16$ kJ/mol calculated by Eq. (20) and does not contradict the estimate made above on the basis of SDDF and the van Willigen model.

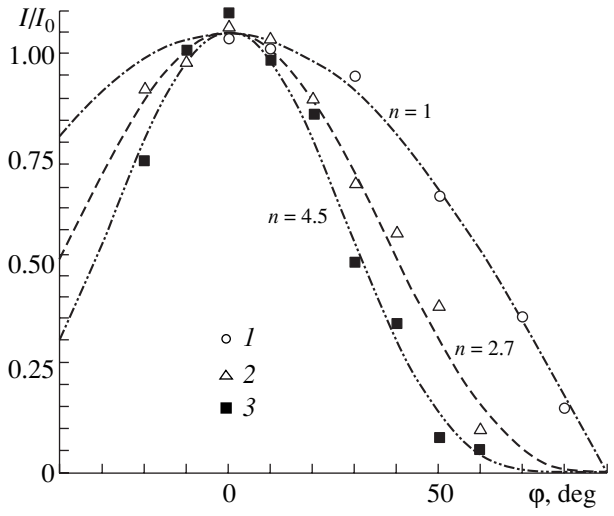

Fig. 18. Spatial distributions of CO flow in the (*1*) molecular desorption and in the reactions (*2*) $C_{ads} + O_{ads} \longrightarrow CO$ and (*3*) $C_{ads} + 1/2O_2 \longrightarrow CO$ on a platinum surface [52, 55]. Dashed lines show the approximation of the experimental data by Eq. (3) with (*1*) $n = 1$, (*2*) 2.7, and (*3*) 4.5.

Carbon dioxide. The dynamics of CO_2 desorption as a product of CO oxidation on the single crystal surfaces of Pt, Pd, Ir, and Rh was studied in more detail than for other gases [5, 20, 26, 60–74].

Normal SDDFs (Table 1) were mainly observed on the (111) faces. In some studies, CO_2 desorption was studied for the (100) surface. Some data are available for the anisotropic Rh(110) surface for which isotropic SDDF of CO_2 was observed [74].

Note that CO_2 SDDFs were measured using two methods: (1) TPR of preadsorbed reactants and steady-state reaction at constant partial pressures of reacting gases and (2) constant-intensity molecular beams.

As in the case of CO and NO desorption, the SDDF of CO_2 molecules from the preadsorbed CO_2 layer followed the Knudsen law [68, 71].

When CO_2 was formed by oxidation reactions, more sharply peaked distributions and higher translational temperatures of desorbing molecules were observed. In these cases, SDDF was often described by Eq. (7) [5, 20, 26, 62, 70, 72, 73].

As can be seen from Table 1, in TPR experiments, the desorption forms of CO_2 were observed at 120–500 K, whereas the steady-state oxidation of CO occurred at $T_{surf} > 450$ K. Although there is some overlap in these temperature ranges (450–500 K), such important parameters as surface concentrations may differ considerably in some experiments carried out by the meth-

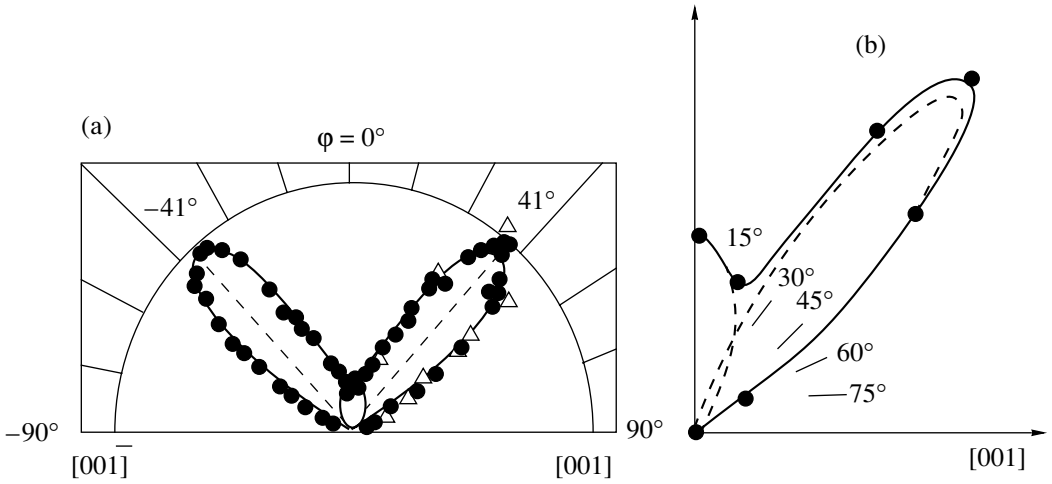

Fig. 19. Spatial distributions of nitrogen molecules desorbing in the decomposition of NO on Pd(110) in the TPR regime according to (a) [88] and (b) [87]. Curves approximating the experimental data (points) are the linear combinations of functions (dashed line) described by Eq. (15) with (a) $n = 28$, $\varphi_0 = 41°$; (b) $n = 46$, $\varphi_0 = 38°$ and Eq. (3) with (a) $n = 5$ and (b) $n = 4.2$.

ods of TPR and steady-state processes. Therefore, we compare similar experiments.

The more sharply peaked distributions observed by the TPR method compared to the steady-state reaction are explained by the higher concentrations of reactants and lower temperatures, which are characteristic of TPR [62].

Unfortunately, few systems were independently studied by different research groups.

A surprising result obtained by Engel and Ertl [60] and demonstrating the applicability of the Knudsen law for the CO/Pd(111) system was not confirmed in a more recent study by Matsushima and coworkers [61–63], who observed the high values of n = (4–8) at approximately the same temperatures and $n = 40$ at lower temperatures.

The greatest number of papers were devoted to CO_2 desorption from Pt(111), but the results obtained by different authors differ substantially. The value of n measured in [5, 26, 66–71] ranges from 6–7 [66, 69, 70] to 13–19 [68]. TPR experiments usually gave higher values of n.

3.2. Anisotropic and Off-Normal Spatial Distributions

Spatial distributions of gases desorbing from stepped single crystal surfaces are much more complex (see Table 3) than those observed on flat surfaces. SDDFs obtained on stepped surfaces provided new information on the dynamics of product formation and surface active sites and their symmetries.

A classical example of anisotropic SDDF was observed for the reactive desorption of CO_2 from Pd(110) [92–94]. Noticeable anisotropy was observed more recently for both SDDF and for the distribution of velocities of molecules desorbing from stepped surfaces [15, 79, 80, 87, 91, 98, 101, 102, 135]. These effects appear due to the anisotropy of the potential of interaction between the surface and a desorbing molecule when the motion of the product molecule along the steps is easy and the motion across the steps is restricted.

As noted above, directed desorption described by Eq. (15) often takes place. In that case, the maximal intensity is observed at a collimation angle φ_0 to the surface normal. The reason for that is the collimation of the desorption flow along the directions of local normals (corresponding to step and terrace planes) rather than to the average normal to the surface [15, 79]. This case is especially interesting from the standpoint of identifying active sites from which reaction products desorb.

Table 3 compiles data on anisotropic and off-normal SDDFs and the velocities of N_2, CO, and CO_2 molecules desorbing from metals.

Nitrogen. Recently, two groups of Japanese researchers published interesting data on N_2 desorption from Pd(110) [81, 87, 88]. For nitrogen formed in NO decomposition in the TPR regime, both groups observed sharply peaked (n = 20–46) symmetric spatial distributions at an angle of ±40° to the global surface normal. This angle virtually coincides with the direction of local normals to inclined (111) terraces (Fig. 19). Simultaneously, a small amount of nitrogen desorbing along the global normal to the surface was observed. Analogous results were obtained for the steady-state reaction $NO_{ads} + CO_{ads} \longrightarrow 1/2\ N_2 + CO_2$ at T_{surf} = 500–620 K [90] (Fig. 20).

In the temperature-programmed decomposition of adsorbed N_2O on Pd(110), almost the same distribution of desorbing nitrogen molecules was observed, although inclined "wings" were narrower ($n = 60$) (Fig. 21) [90], which is probably explained by the lower temperature (152 K) of the process. The fact that

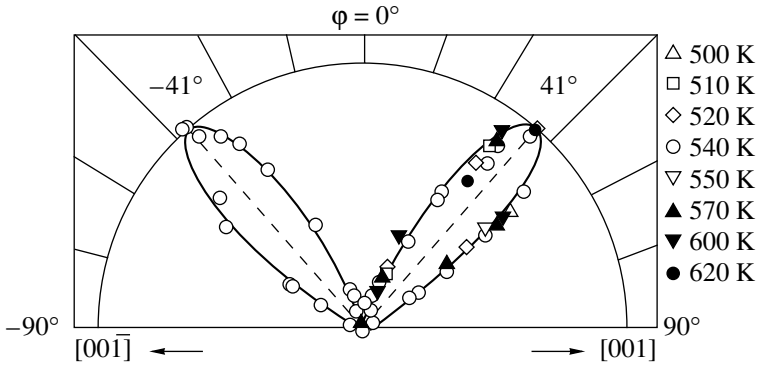

Fig. 20. SDDF of N_2 molecules in the [001] plane observed in the course of the steady-state reaction NO + CO ⟶ $1/2N_2 + CO_2$ on Pd(110) at the reactant pressures $P_{NO} = 2 \times 10^{-8}$ torr and $P_{CO} = 1 \times 10^{-8}$ torr and different temperatures [90].

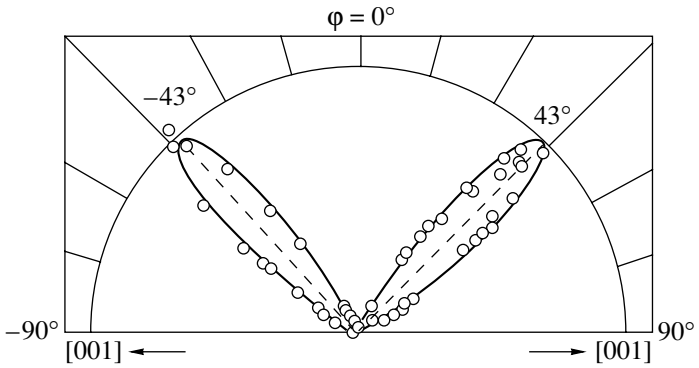

Fig. 21. SDDF of β_1-N_2 in the TPR regime from Pd(110) after the preliminary adsorption of N_2O [90].

SDDFs of nitrogen observed in three reactions are almost identical suggests that N_2O_{ads} is an intermediate product of NO decomposition formed by the recombination of NO_{ads} and N_{ads} [89].

Nitrogen molecules formed in the reaction $N_2O_{ads} \longrightarrow N_2 + O_{ads}$ have a high energy because the process is highly exothermic, $\Delta H \approx -190$ kJ/mol [135].

Direct measurements of the velocity distributions of nitrogen molecules [88, 90] formed on Pd(110) in three processes (TPR of decomposition $2NO_{ads} \longrightarrow N_2 + O_2$, $N_2O_{ads} \longrightarrow N_2 + O_{ads}$, and the steady state reaction $6NO + 4CO \longrightarrow N_2 + 2N_2O + 4CO_2$) revealed a unique effect: two fast components with T_{tr} = 580 and 1930 K [89] (Fig. 22). Kobal and Matsushima [89] assumed that these components correspond to the first and ground vibrational levels of the nitrogen molecule differing in energies by 0.28 eV. Thus, the total energy of the N_2 molecule is distributed between the vibrational and translational degrees of freedom: the higher value of one of the energy types corresponds to the lower value of the other.

The SDDF of $^{14}N^{15}N$ formed in the reaction $^{15}N_{ads} + {}^{14}NO_{ads} \longrightarrow {}^{14}N^{15}N + O_{ads}$ at 460 K on Pd(110) was directed at angles ±38° to the global surface normal in the direction [001], although the recombinative desorption of $^{15}N_2$ only observed at temperatures higher than 600 K was directed along the normal to the surface and described by Eq. (3) with n = 6–7 [87].

These facts provide evidence for the fact that the recombinative desorption of nitrogen occurs on the bottom of "trenches" or on the "ridges" of stepped surfaces, whereas the formation of N_2 in the decomposition of N_2O_{ads} occurs via another pathway. One could assume that, in the second case, the reaction occurs on inclined terraces. However, in the regime of the steady-state reaction $6NO + 4CO \longrightarrow N_2 + 2N_2O + 4CO_2$, the SDDF of CO_2 is directed along the normal to the surface, pointing to the fact that the Pd(110) is not reconstructed (the steps are too narrow to lead to collimated desorption). However, in this case, nitrogen desorption occurs at the same angles as in the case of N_2O decomposition (Figs. 20 and 21).

Matsushima and coworkers [88–90] proposed the following interesting mechanism of collimated desorption of nitrogen in the decomposition of N_2O. They assume that the N_2O molecule is positioned across the steps on Pd(110) as shown in Fig. 23. When the N–O bond dissociates, the oxygen atom moves from a ridge

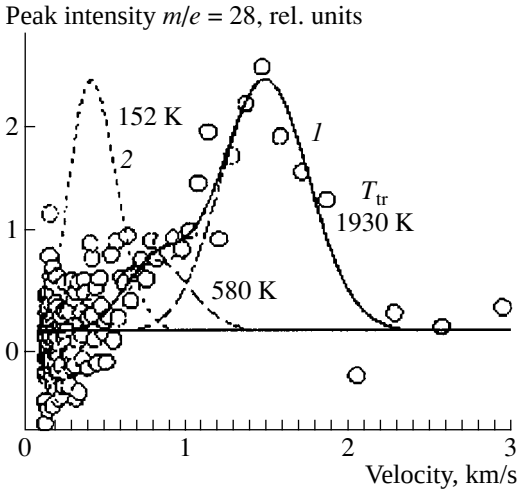

Fig. 22. (*1*) Distributions of desorbing N_2–β_1 molecules ($\varphi = 43°$) from Pd(110) and (*2*) the Maxwell distribution at $T = T_{surf} = 152$ K [89].

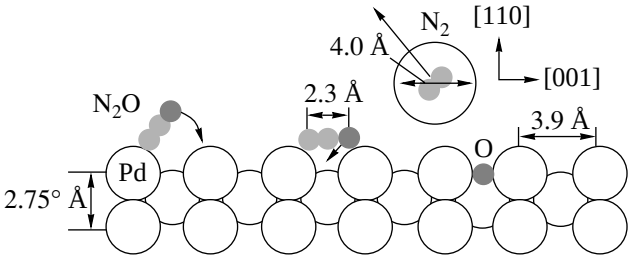

Fig. 23. N_2O binding to Pd(110) [89].

to the bottom of a trench and imparts additional momentum to an N_2 molecule in the direction [001], resulting in N_2 desorption in the off-normal direction.

Ikai and Tanaka also measured nitrogen SDDF on Pd(211) [91] and Rh(533) [82] in the TPR regime of reactions $2N_{ads} \longrightarrow N_2$, $N_{ads} + NO_{ads} \longrightarrow N_2 + O_{ads}$, and $2NO_{ads} \longrightarrow N_2 + O_2$. As in the case of the Pd(110) surface, desorption along the surface normal in the recombination of nitrogen atoms and the directed desorption of nitrogen were observed in two processes.

Nitrogen monoxide. Tanaka and coworkers [45] obtained interesting results for the recombinative desorption of NO on Ag(110). The desorption at an angle of 17° to the surface normal was observed in the [001] plane parallel to the steps, although in the perpendicular [110] plane, SDDF had a maximum in the direction of the surface normal (Fig. 24). Note that in all other cases described in this section, the opposite picture was observed. This is explained by the deviation of local step normals from the global surface normal.

The authors of [45] explain this unexpected result as follows. As they have shown earlier [136] by STM, oxygen adsorbed on Ag(110) forms $(–Ag–O–)_n$ rows. The recombination of nitrogen and oxygen atoms may occur in two ways (Fig. 25): the recombination of nitrogen with oxygen atoms inside the row and with terminal oxygen atoms. In the former case, oxygen atoms are bound with two silver atoms and form a symmetric structure in the direction [001], and the desorption of NO occurs in the direction of the surface normal. In the second case, oxygen is bound to only one silver atom and the structure becomes asymmetric in the [001] direction, resulting in the off-normal emission of NO.

Carbon monoxide. Recent results obtained by Walker and King [84] for CO SDDF in the reaction $C_{ads} + 1/2O_2 \longrightarrow CO$ on Pt(110)(1 ± 2) at 650 K are shown in Fig. 26. This spatial distribution has two sharp symmetric peaks directed at angles ±32° to the global surface normal and approximated by the expression $\cos^{50}(\varphi \pm 32)$. Some small contribution of the cosine Knudsen distribution is also observed. It is likely that the reaction mainly occurs on inclined terraces.

Carbon dioxide. The anisotropic and directed desorption of CO_2 formed in CO oxidation on stepped surfaces was mostly studied by Matsushima and coworkers [14, 15, 79, 80, 83, 85, 86, 90, 94, 96, 98–104, 135].

The anisotropic SDDFs of CO_2 were first observed in CO oxidation on Pd(110) [14]. Analogous results were obtained on the unreconstructed Ir(110)(1 × 1) surface [80]. In both cases, narrow distributions in the plane perpendicular to the steps and broader distributions in the direction parallel to the steps were observed. On the other hand, in the desorption of CO_2 from Rh(110), SDDF anisotropy was detected for none of the desorption forms at 170–500 K [74].

The spatial distributions of CO_2 molecules desorbing from reconstructed Ir(110)(1 × 2) [80] and Pt(110)(1 × 2) [15, 94, 98] surfaces were more complex. They had two anisotropic maximums at angles of ±23°–25° to the surface normal in the plane perpendicular to the steps. Moreover, under some conditions, desorption along the normal to the surface was observed. These reconstructed surfaces consist of narrow (111) terraces. These microfacets are inclined in opposite directions at ±35° to the (001) axis [15, 94]. The maximums of SDDF were observed in directions that are close to the local normals of the terraces. These maximums are anisotropic: they are narrow in the plane perpendicular to the steps and broader in the parallel direction.

Figure 27 shows data on the above reaction under steady-state conditions on Pt(110) [98]. In the steady-state reaction of CO oxidation, the so-called kinetic transition [137] is observed at certain critical pressures of CO. At a critical pressure, the reaction rate drastically decreases, and CO retards the process at higher pressures. The range below the critical pressure is called active, and the range above the critical pressure is called inhibited. At the critical pressure, the effect of site switching is observed. In the active zone (at low CO pressures), the reaction largely occurs on the inclined terraces of the reconstructed Pt(110)(1 × 2) surface as is evident from collimated CO_2 desorption. In the inhib-

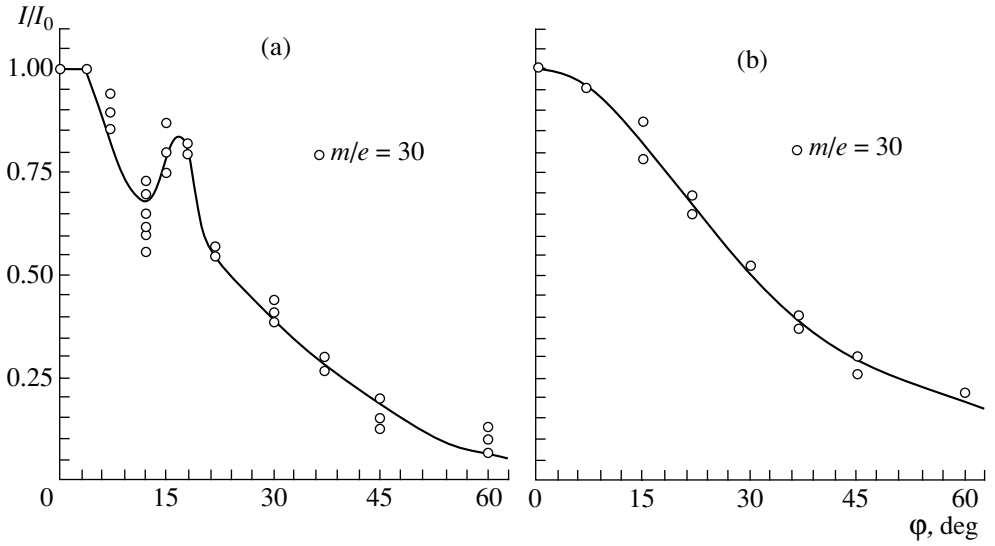

Fig. 24. Spatial distribution of NO molecules desorbing from the [$p(2 \times 3)$-N+ $p(2 \times 1)$-O]Ag(110) at 520 K in the directions (a) [001] and (b) [110] [45].

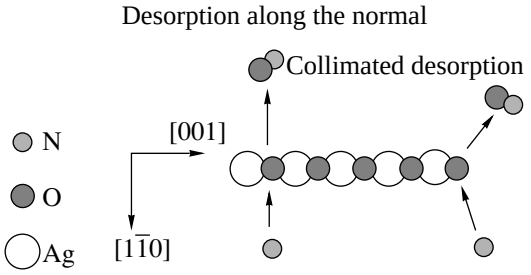

Fig. 25. Two pathways of the reaction of nitrogen atoms with terminal and nonterminal oxygen atoms in the $(-Ag-O-)_x$ sequences [45].

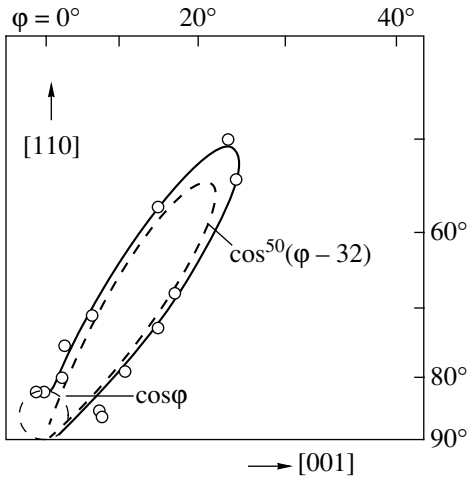

Fig. 26. SDDF of CO formed in the reaction $C_{ads} + O_{ads} \longrightarrow$ CO on Pt(110)(1 × 2) at T_{surf} = 650 K [84]. The solid line approximating the experimental data is a linear combination of functions described by Eq. (15) with $n = 50$, $\varphi_0 = 32°$ and Eq. (2).

ited range after the critical transition, the SDDF of CO_2 drastically changes and becomes directed along the normal to the surface. This is probably explained by surface reconstruction to form the Pt(110)(1 × 1) pattern and the occurrence of the reaction at the bottom of trenches. Figure 28 illustrates the formation of CO_2 on the reconstructed and unreconstructed Pt(110) surfaces.

Recently, a series of papers have been published on the formation of CO_2 on the stepped surfaces of Pt(113) [83, 85, 100–102], Pt(112) [99, 135], and Pt(557) [104]. These surfaces are characterized by monatomic steps (001) and terraces (111) of different widths: (113) = (*s*)2(111) × (001), (112) = (*s*)3(111) × (001), and (557) = (*s*)6(111) × (001).

The results obtained on these three surfaces by the space-resolved TPR method have general features. The spatial distributions of desorbing CO_2 molecules from these surfaces are anisotropic, asymmetric, and inclined to the surface normal. They depend on the azimuthal angle and on the surface concentrations of reactants (θ_{CO} and θ_O). The SDDF in the plane parallel to the steps is directed along the normal to the surface. It becomes sharper with an increase in the surface concentrations of CO and oxygen, and the value of n increases from ~6 to ~14 [101, 102, 135].

The distributions in the plane perpendicular to the steps observed on Pt(112) at different θ_{CO} and at a temperature of 400 K [99] are asymmetric at low θ_{CO} or high θ_O and can be approximated by the equation $I/I_0 = \delta\cos^8(\varphi + 25) + \nu\cos^{12}(\varphi - 10)$ (where δ and ν are constant coefficients. Thus, CO_2 desorption is collimated along the directions close to the local normals of terraces (111) and steps (001).

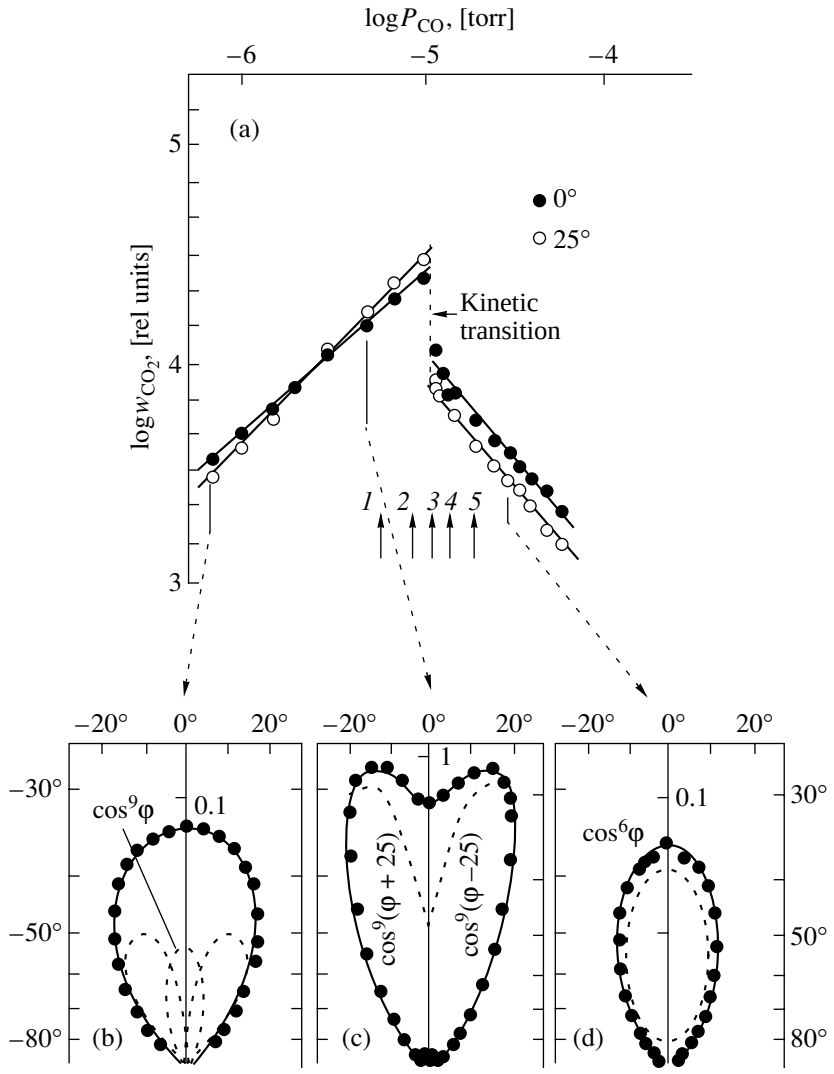

Fig. 27. (a) Dependence of CO_2 desorption formed in the steady-state reaction on Pt(110) on the CO pressure observed at $\varphi = 0°$ and 25°, $P_{O_2} = 3 \times 10^{-5}$ torr, and $T_{surf} = 500$ K. Vertical arrows with numbers point to the position of the kinetic transition at T_{surf} (*1*) 460, (*2*) 480, (*3*) 500, (*4*) 550, and (*5*) 600 K. (b–d) Spatial distributions of CO_2 in the (001) plane in the polar coordinates. Dashed lines show the position of SDDF with cosine functions, and solid lines show the sum of components. Dashed arrows show CO pressures at which measurements were carried out: (b) 7×10^{-7}, (c) 5×10^{-6}, and (d) 3×10^{-5} torr [98].

On the Pt(557) surface [104], two processes of CO_2 formation were found. These are the reactions of adsorbed CO molecules with adsorbed oxygen atoms at 200–500 K and with oxygen molecules at temperatures below 200 K. In the first process, CO_2 desorption is collimated along the direction that is close to the local normals of terraces (111). In the second process the direction is opposite with an angle of 7° relative to the global normal. These data suggest that the two cited processes occur on different active sites.

The SDDFs of CO_2 on the Pt(113) surface were measured both under TPR conditions [100–103] and in the steady-state oxidation of CO [83, 85]. The SDDFs of CO_2 heavily depend on the CO pressure and have completely different shapes in the active and inhibited ranges of the steady-state process (Fig. 29). In this case, we clearly see the effect of site switching. Figure 30 shows the structure of unreconstructed (Pt(113)(1 × 1)) and reconstructed (Pt(113)(1 × 2)) surfaces. In the active range, collimated desorption of CO_2 at an angle of +22° to the surface normal is observed, which roughly coincides with the local normal to the terraces (111) (+29.5°). In the inhibited range, collimated desorption is mostly observed at an angle of –20°, which is close to the direction of the local normal to steps (001) (–25.2°). In the general case, SDDF in the plane perpendicular to the steps is approximated by the linear combination of functions $\cos^7(\varphi - 22)$ and $\cos^7(\varphi + 20)$.

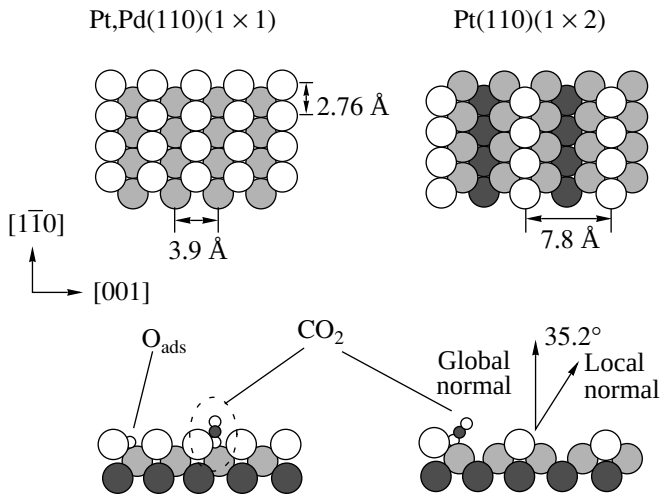

Fig. 28. The formation of CO_2 on Pt,Pd(110)(1 × 1) and Pt(110)(1 × 2).

As can be seen from the above examples, the SDDFs of CO_2 molecules formed in CO oxidation are rather sensitive to the structure of stepped surfaces and provide information on the active sites of the surface.

Let us consider the conditions under which information on the surface structure can be obtained from the SDDF of CO_2 molecules.

The physical adsorption of CO_2 on the surface of noble metals occurs at temperatures below 110 K, and the equilibrium distance of the adsorbed molecule from the surface is ~3 Å. The CO_2 molecule formed by the reaction between CO and O should be repulsed by the surface. This is associated with the fact that chemisorbed reactants and the activation barrier are much closer to the surface than the physically adsorbed CO_2 molecule. The CO_2 molecule has an almost ellipsoidal shape, 3.8 Å in width and 5.2 Å in length; that is, steps and terraces that are 3.8 Å in width will hardly shift the collimation angle of CO_2 desorption from the global surface normal.

Indeed, the SDDF of CO_2 formed on the unreconstructed stepped surfaces of Pt(110), Pd(110), Rh(110), and Ir(110) are directed along the global normal to the surface, because the width of steps in this case is too small.

On the other hand, on the Pt(110)(1 × 2), Ir(110)(1 × 2), Pt(112), Pt(113), and Pt(557) surfaces, the desorption of CO_2 is collimated in the directions to the local normals of terraces. In these cases, except for Pt(113), the width of inclined terraces (111) is three atoms or more. Thus, we may assume that the width of three atoms is minimal for the collimated desorption of CO_2 in the direction of the local normal. This also explains the difficulties in detecting CO_2 desorption from monatomic steps, although the reaction can occur on these steps.

3.3. Three Most Important Characteristics of Desorption of Translationally Excited Molecules

Based on numerous experiments, Matsushima formulated three physical characteristics, which can be determined from SDDF measurements and the measurements of kinetic energies of reactively desorbed CO_2 molecules [7].

The effect of reactant surface concentrations on SDDF was first observed for CO_2 formed on Rh(111) in the TPR regime [20]. More recently, it was shown that this phenomenon is typical of the reactive desorption of CO_2 on other surfaces: Pd(111) [62, 63], Pd(100) [64], Pd(110) [93], and Rh(110) [74]. On these surfaces, several TPR peaks were observed. The lower the peak temperature, the sharper the SDDF of CO_2 and the higher T_{tr} (Fig. 31 and Tables 1 and 3).

One could assume that this effect is due to the surface temperature, but the van Willigen model (Eq. (20)) predicts the opposite result: a small linear increase in T_{tr} with an increase in T_{surf}, which was experimentally conformed in the steady-state reactive desorption in several systems: D_2/Ni(100) [37], N_2/Rh(111) [9], NO/Rh(111) [59], CO_2/Pt(111) [70], CO_2/Pt(133) [138], and CO_2/Pd(110) [97]. Thus, the surface temperature cannot explain this effect.

Matsushima provided other explanation based on the lateral interactions in the overlayer. With an increase in the surface concentration of reactants, the lateral interactions increase and product CO_2 molecules experience greater repulsion from the surface, resulting in more sharply peaked SDDFs and higher kinetic energies of desorbing CO_2 molecules.

SDDF anisotropy and the distribution of the velocities of desorbing molecules are also important characteristics of the reactive desorption of translationally excited molecules. This is due to a certain symmetry of

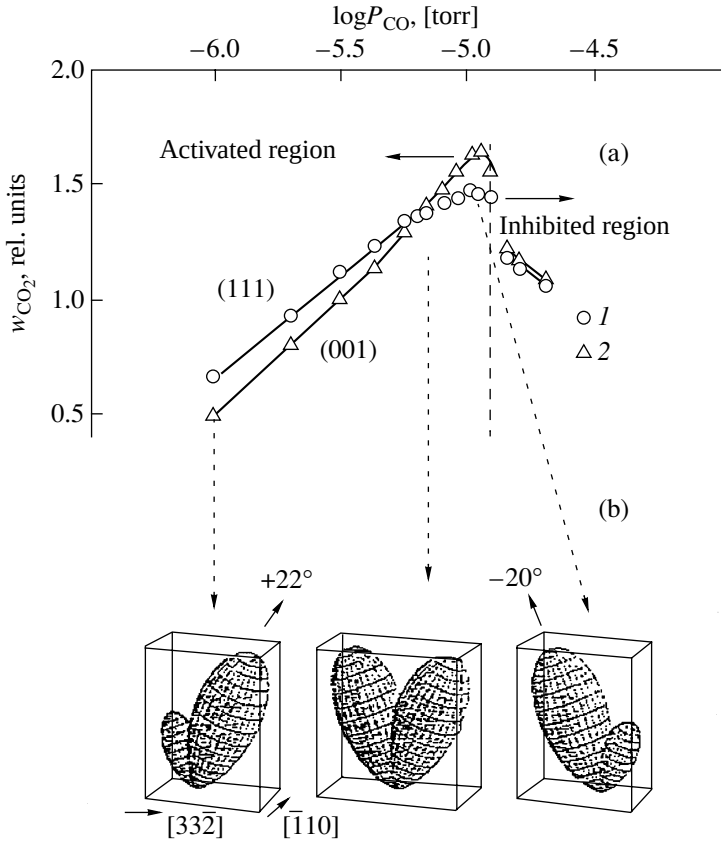

Fig. 29. (a) Dependence of the rate of CO_2 (w_{CO_2}) formation on (*1*) terraces (111) and (*2*) steps (001) of Pt(113) on P_{CO} under steady-state conditions at 573 K and $P_{O_2} = 3 \times 10^{-5}$ torr [83]. The dashed straight line shows the kinetic transition. (b) 3D image of the CO_2 SDDF in polar coordinates.

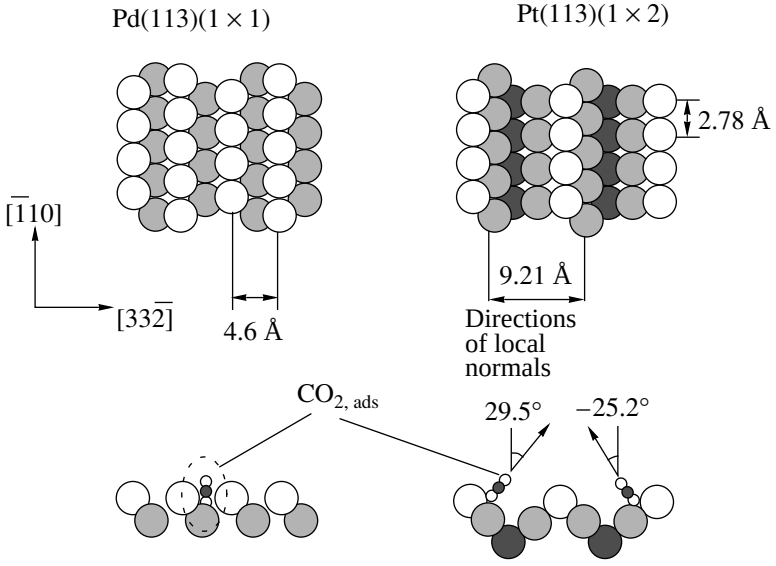

Fig. 30. CO_2 formation on Pt(113)(1 × 1) and Pt(113)(1 × 2).

active sites on a number of stepped surfaces (Table 3). It was not detected on flat surfaces.

In the oxidation of carbon monoxide on platinum-group metal surfaces, the diffusion of adsorbed CO molecules to adsorbed oxygen atoms probably occurs, because the mobility of CO is much higher than the mobility of oxygen atoms [139]. Therefore, the formation of CO_2 occurs at the sites of oxygen adsorption.

On the unreconstructed Pd(110) surface, chemisorbed oxygen is between three palladium atoms [140, 141], as shown in Fig. 28. These sites are open in the direction along the steps and shielded by palladium atoms in the perpendicular direction. Such an environment probably causes the anisotropy of the momentum of a desorbing CO_2 molecule, because its motion in the perpendicular direction to steps is constrained. The same mechanism explains the anisotropy of SDDF observed in CO_2 desorption from sites on the terraces of stepped surfaces.

The orientation of active sites was first deduced from the SDDF of CO_2 from the reconstructed Pt(110)(1 × 2) surface [15]. Indeed, this surface is especially convenient for studying the orientation of active sites, because it consists of terraces with the (111) structure and terrace normals deviate from the global surface normal to the opposite sides along the direction [001] (see Fig. 28).

On this surface, four TPR peaks were observed for CO_2 in the temperature range 170–400 K and the SDDF of CO_2 at low surface concentrations of CO (high temperatures) has two maximums at ±24° with respect to the global normal in the plane perpendicular to the steps [94].

The translational temperature under these conditions also reaches a maximum at collimation angles corresponding to the maximum of the desorption flow, and $T_{tr} \gg T_{surf}$. This fact is evidence for the desorption of translationally excited molecules.

These data suggest that the reaction occurs on inclined terraces (111) where oxygen atoms are adsorbed. The sites for oxygen adsorption are between three platinum atoms [15, 142, 143] as on the flat Pt(111) surface [144–146].

On the other hand, at high surface concentrations (low temperatures), the analysis of SDDF reveals the presence of another anisotropic component whose maximum of the desorption flow is observed in the direction of the global surface normal [15, 142, 143]. This carbon dioxide is formed on the bottom of surface "furrows".

If the structure of the platinum single crystal surface is ideal, then triatomic terraces (111) on Pt(110)(1 × 2) should be inclined to the angles of ±35° relative to the plane of this surface. In fact, the upper atoms are shifted toward the bulk, and the atoms of the second layer are shifted parallel to the surface, and the angle of terraces

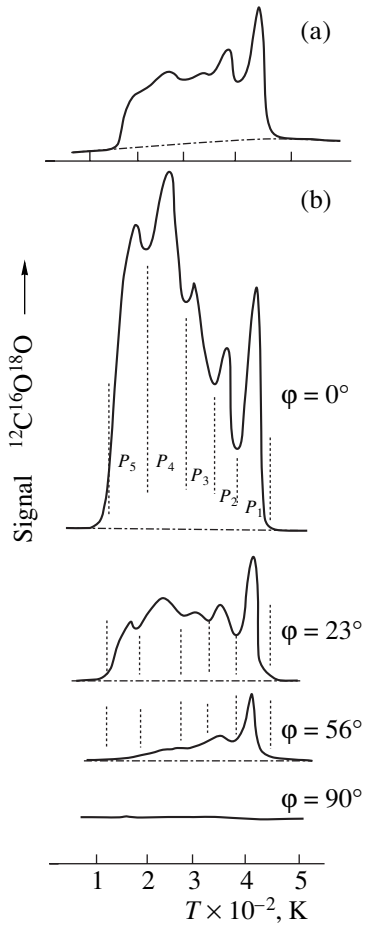

Fig. 31. The TPR spectrum of CO_2: (a) integral and (b) space-resolved in the [001] direction observed on Pd(110) at different initial coverages $\theta_O = 0.45$ and $\theta_{CO} = 0.5$ and a heating ramp of 15 K/s [93].

is ±30° [147], which is somewhat higher than the value ±24° obtained from SDDF analysis.

Noticeable deviations of collimation angles from local normals were also found on other stepped surfaces: Ir(110)(1 × 2) [79, 80], Pt(112) [99, 135], Pt(113) [83, 85, 100–102], and Pt(557) [104]. The values of the corresponding collimation angles and the angles of terrace (111) inclination are shown in Fig. 32. As can be seen from this plot, the collimation angles systematically deviate to an angle of ~30% (curve *1*) from local normals toward lower values corresponding to the ideal crystal (curve *2*). Consideration of surface atomic shifts makes it possible to decrease these deviations (curve *3*), but a difference of ~15% remains. This difference can be explained by the smoothing effect of conductance electrons [148].

Thus, the SDDF of collimated desorption makes it possible to identify the portions of the surface (active sites) on which reaction products are formed.

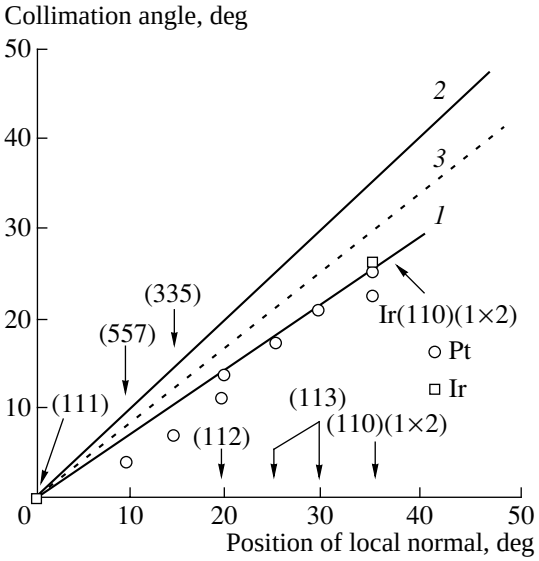

Fig. 32. Dependence of the collimated CO_2 desorption angle on the direction of local normals on stepped platinum and iridium surfaces. Points and line *1* show the experiment; line *2* show data for an ideal lattice [7], and line *3* show data taking into account lattice distortion.

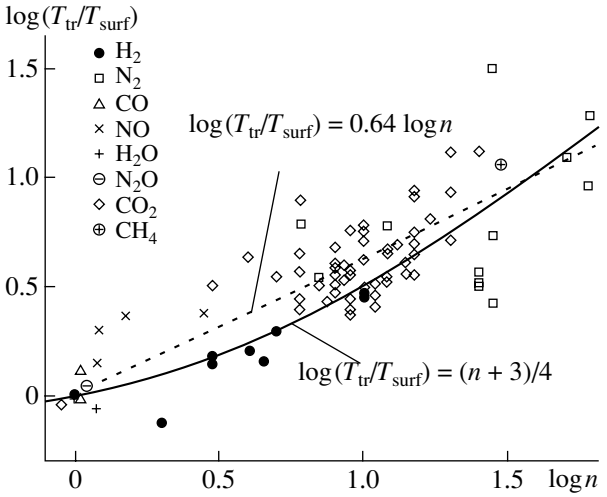

Fig. 33. Correlation of SDDF (n in Eqs. (3), (*7*), (*15*)) with the ratio of the translational temperature of desorbing molecules to the surface temperature (T_{tr}/T_{surf}) (dashed line) obtained on the basis of experimental data (points) [4–6, 9, 10, 26, 28, 37–40, 47, 49, 59, 61, 65, 70, 72, 73, 75, 83, 85, 86, 88–90, 92–105]. The solid line is described by Eq. (21) based on the van Willigen model.

3.4. Correlation of Spatial Distributions and Translational Energies of Desorbing Molecules

Obviously, sharply peaked SDDFs and the high translational temperatures of desorbing molecules are due to the repulsion of products from the catalyst surface. Therefore, we would expect there to be some relations between these phenomena. As we showed above, simple relation (21) between $T_{tr\perp}/T_{surf}$ and the parameter n that characterizes SDDF can be derived from the Van Willigen model.

Much experimental data have been obtained on SDDF and T_{tr} for various gases (see Tables 1 and 3). These data are shown in Fig. 33 in the logarithmic coordinates $\log(T_{tr\perp}/T_{surf}) - \log n$. For collimated desorption, the maximal values of the translational temperature measured at the collimation angle are given for $T_{tr\perp}$. The linear approximation

$$\log(T_{tr\perp}/T_{surf}) = 0.64\log n \qquad (23)$$

is shown by a dashed line. The solid line shows the results of calculations by Eq. (21).

Both curves adequately describe the experimental data. Only a few points characterized by a low accuracy of measurements noticeably deviate from the correlation dependence.

The solid line corresponding to Eq. (21) describes data on hydrogen desorption especially accurately.

Thus, there is a clear correlation between the spatial distribution of desorbing molecules and their kinetic energies, and this correlation is close to that predicted by the van Willigen model.

Equations (21) and (23) can be used for making estimates of $T_{tr\perp}$ on the basis of n or vice versa.

3.5. Distribution of Energy over the Degrees of Freedom of Desorbing Molecules

Information on the excited states of various degrees of freedom of molecules during their desorption is very important for understanding the process dynamics. Unfortunately, information on the excitation of internal degrees of freedom is scarce. All results obtained to date are collected in Table 4. Only two papers [9, 49] devoted to nitrogen desorption contain information on energies of all three types (translational, vibrational, and rotational) for desorbing molecules. In all other cases, we have to compare data on translational and internal energies taken from different sources.

Nevertheless, analysis of these results provides some general insights. Under comparable conditions, translational, vibrational, and rotational temperatures (energies) decrease in the following series:

$$T_{tr} \geq T_{vib} > T_{rot}. \qquad (24)$$

Usually, the rotational energy is close to the surface temperature or even lower [49, 145, 151]. The fraction of translational energy in the general balance may be 40–80%.

Rettner *et al.* [112] carried out a complex study of the dynamics of adsorption/desorption for the H_2/Cu(111) system. Using the principle of microscopic reversibility and the results of experiments on desorption, they found the dependence of the initial sticking probability (S_0) on the kinetic energy of collision (E_i)

Table 4. Translational, vibrational, and rotational temperatures of desorbing molecules

System	Methods and processes	T_{surf}, K	T_{tr}, K	T_{vib}, K	T_{rot}, K	Ref.
D_2/Ag(111)	TPD					
	$2D_{ads} \longrightarrow D_2$	190	522	–	–	[27]
	MB, REMI	210	–	–	430 ± 50	[149]
	$2D \longrightarrow D_2$	293	–	800 ± 100	–	
H_2, D_2/Cu(111)	DMM, VM					[28]
	$2H_{ads} \longrightarrow ç_2$	1000	4000	–	–	
	$2D_{ads} \longrightarrow D_2$	1000	4000	–	–	
	DMM, REMI					[150]
	$2D_{ads} \longrightarrow D_2$	850	–	$T_{vib} > T_{surf}$	$T_{rot} > T_{surf}$	
N_2/Cu(111)	SSCR, VM, REMI					[10]
	$2N_{ads} \longrightarrow N_2$	700	21000	5100	800–900	
N_2/Ru(001)	SSCR, VM, RBPI					[49]
	$2NH_3 \longrightarrow N_2 + 3H_2$	900	3150	≈3000	630	
CO_2/Pd(111)	SSCR, VM					[61]
	$CO + 1/2O_2 \longrightarrow CO_2$	500–823	1750–2500	–	–	
	VM, SSCR, FTIR					[151]
	$CO + 1/2O_2 \longrightarrow CO_2$	650–850	–	1600–2340	1130–1400	
CO_2/Pd(110)	SSCR, VM					[97]
	$CO + 1/2O_2 \longrightarrow CO_2$	500–700	3500–4000	–	–	
	VM, SSCR, FTIR					[152]
	$CO + 1/2O_2 \longrightarrow CO_2$	650	–	1300	960	
CO_2/Pd(100)	SSCR, VM					[61, 65]
	$CO + 1/2O_2 \longrightarrow CO_2$	550–700	1500–2100	–	–	
	VM, SSCR, FTIR					[153]
	$CO + 1/2O_2 \longrightarrow CO_2$	650	–	1530	1150	
CO_2/Pt(111)	MB, SSCR, VM					[26]
	$CO + 1/2O_2 \longrightarrow CO_2$	800	3200	–	–	
	VM, SSCR, FTIR					[151]
	$CO + 1/2O_2 \longrightarrow CO_2$	870	–	1580	700	

Note: FTIR—Fourier-transform infrared spectroscopy; RBPI—resonance biphoton ionization; REMI—resonance-enhanced multiphoton ionization; for other abbreviations, see Table 1.

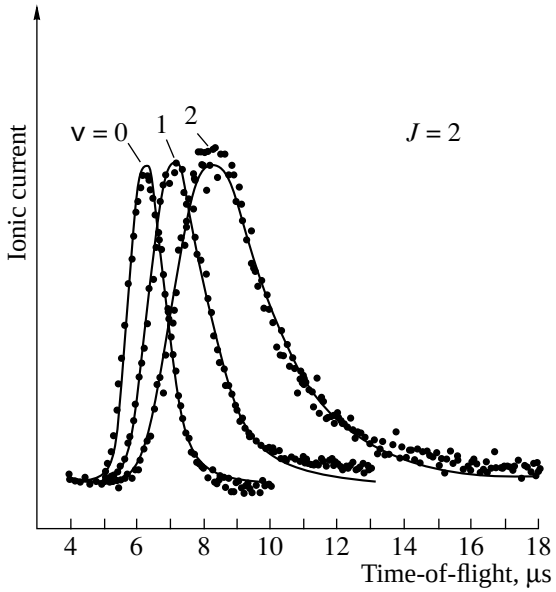

Fig. 34. Time-of-flight distributions of deuterium molecules desorbing from Cu(111) with the resolution over vibrational and rotational levels for $v = 0, 1, 2$; $J = 2$; $T_{surf} = 925$ K [30].

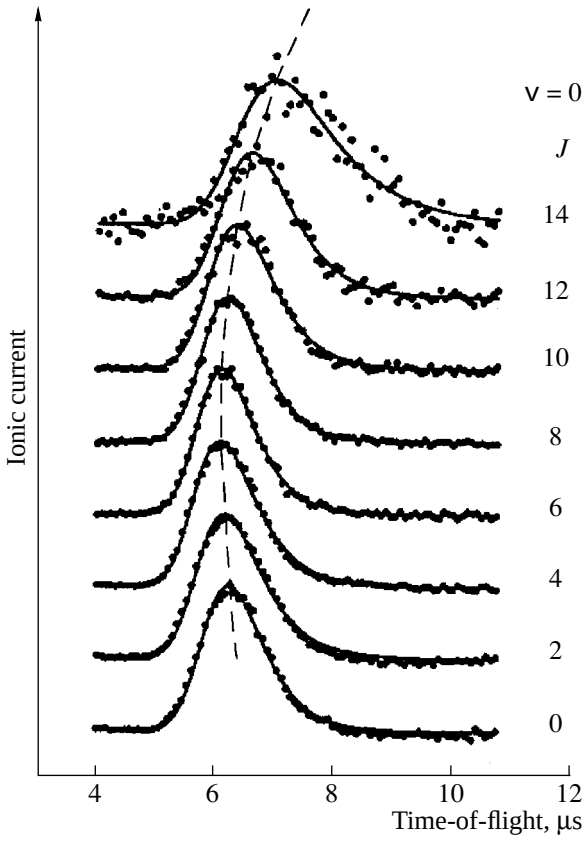

Fig. 35. Time-of-flight distributions of deuterium molecules desorbing from Cu(111) with the resolution over rotational levels for the ground vibrational state. $T_{surf} = 925$ K [30].

for various vibrational and rotational quantum states of a hydrogen molecule. These experiments provided detailed information on the quantum levels $J = 0$–10 at $v = 0$ and $J = 0$–7 at $v = 1$ (J and v are rotational and vibrational numbers, respectively). Figures 34 and 35 show the results of the time-of-flight measurements of D_2 molecules desorbing from the Cu(111) surface in various quantum states [30].

In direct experiments on the dissociative adsorption of beamed H_2 molecules, Rettner *et al.* [112] measured S_0. It was found that S_0 depends on the normal translational energy, $E_\perp = E_i\cos^2\varphi_i$, where φ_i is the angle between the beam and the surface normal. Molecular beam experiments provided additional information on the dependence of the H_2 ($v = 2$) sticking probability on J. The results of these measurements are described by the empirical s-shaped function of the form

$$S_0 = G\{1 + \mathrm{erf}[(E_\perp - E_0)/W]\}/2. \qquad (25)$$

Parameter W determines the width of the transition portion on the curve. The value of G is insensitive to v and J but depends on $E_\perp$. The apparent activation energy E_0 determining the position of the inflection point on the curve does depend on v and J. For instance, E_0 for H_2 ($v = 0$) molecules is ~0.6 eV and decreases to 0.3 and 0.1 eV for H_2 ($v = 1$) and H_2 ($v = 2$). Thus, there is some compensation of the translational energy at the expense of the vibrational energy. For the process of dissociative adsorption, the first is twice as efficient as the second. The rotational quantum states of the hydrogen molecule slightly affect the value of E_0. It increases insignificantly with an increase in J (at $J < 4$) and then decreases at $J > 4$.

4. ELEY–RIDEAL REACTIONS

The dynamics of product desorption in these reactions is much less studied than the processes occurring in the adsorbed layer via the Langmuir–Hinshelwood mechanism.

In this field, only several papers by Rettner and coworkers are known [5, 16, 17] where the spatial distributions of products formed by the reactions of atomic beams of hydrogen and deuterium directed at an angle to the surface with adsorbed H, D, and Cl atoms and $CH_3^{\cdot}$ and $CD_3^{\cdot}$ radicals are studied. In these studies, the translational, vibrational, and rotational temperatures (T_{tr}, T_{vib}, and T_{rot}) of desorbed molecules were measured or estimated. The results are summarized in Table 5.

As can be seen from this table and Figs. 36–38, the SDDF peaks are shifted relative to the normal in the direction of the atomic beam velocity component that is parallel to the surface. The distribution of energy over the degrees of freedom of product molecules are characterized by inequalities similar to (24):

$$T_{tr} > T_{vib} > T_{rot}, \qquad (26)$$

Table 5. Dynamic parameters of the Eley–Rideal reaction with the spatial distribution of desorbing products

System	Methods and processes	E_{beam}, eV	n	φ_0, deg	T_{surf}, K	T_{tr}, K	T_{vib}, K	T_{rot}, K	Ref.
HD/Cu(111)	MB, VM, MPI								[16]
	$H + D_{ads} \longrightarrow HD$	0.07	8 ± 1*	2*	100	5600 ± 1000	3050 ± 250	1900 ± 250	
	$D + H_{ads} \longrightarrow HD$	0.07	2.0 ± 0.3*	3*	100	6600 ± 500	3300 ± 250	1800 ± 250	
HCl/Au(111)	MB, VM, REMI	0.07	15 ± 2*	6*	100	2540 ± 250	–	–	[6]
	$H + Cl_{ads} \longrightarrow HCl$	0.3	20 ± 2*	8*	100	2840 ± 250	–	–	
		–	–	–	300	3050	1625	560	
CD_4/Cu(111)	MB, VM								[17]
	$D + CD_{3,\,ads} \longrightarrow CD_4$	0.07	60	1.5	95	9150 ± 1000	>4400**	<870**	
CH_4/Cu(111)		0.25	70	5.5	95	9900 ± 1000	–	–	
	$H + CH_{3,\,ads} \longrightarrow CH_4$	0.25	60	3.5	95	11200 ± 1500	–	–	

Note: MPI is multiphoton ionization, E_{beam} is the kinetic beam energy. For other abbreviations see text and Table 1. SDDFs are approximated by the equation $I/I_0 = \cos^n(\varphi - \varphi_0)$.

* Author's estimate.

** Theoretical estimate [17].

and the translational energy constitutes more than 50% of the full energy.

Reactions $H + D_{ads} \longrightarrow HD$ and $D + H_{ads} \longrightarrow HD$ on Cu(111). The spatial distributions of HD formed in these processes at T_{surf} = 100 K and the kinetic energies of atomic beams E_{beam} = 0.07 and 0.30 eV are shown in Fig. 36 [16]. These distributions are asymmetric relative to the surface normal and depend on the kinetic energy of beamed atoms E_{beam}. This fact points to the effect of momentum parallel to the surface. A substantial kinetic isotope effect is observed. At high beam energies, the distributions become bimodal and desorption occurs at two different collimation angles. The HD molecules are very excited over all degrees of freedom, and their full energy is close to the reaction heat, which is equal to 2.3 eV.

Reaction $H + Cl_{ads} \longrightarrow HCl$ on Au(111). Figure 37 shows the results of velocity measurements of HCl molecules [6]. At low temperatures, only high-energy molecules are observed, whereas at T_{surf} > 170 K, the distributions over the velocities become bimodal. The emission of low-energy molecules corresponds to their formation via the Langmuir–Hinshelwood mechanism, and their translational temperature is close to T_{surf}. The spatial and velocity distributions measured at T_{surf} < 170 K point to the occurrence of the reaction via the purely Eley–Rideal mechanism: a sharp asymmetric peak is observed, and the translational temperature of the product molecules is much higher than the surface temperature (Figs. 37 and 39). Moreover, the angle between the surface normal and the direction of emission of desorbing molecules increases with an increase in the beam energy. The full energy of desorbing HCl molecules is approximately equal to half the reaction heat.

Reactions $D + CH_{3,\,ads} \longrightarrow CD_4$ and $H + CH_{3,\,ads} \longrightarrow CH_4$ on Cu(111). These systems show very sharp spatial distributions of desorbing products (Fig. 38) [17]. The deviation of the SDDF peak from the surface normal depends on the atomic beam energy and on their mass. For these reactions and the respective conditions, the authors of [17] theoretically calculated these deviations based on the conservation of momentum in the direction parallel to the surface.

For deuterium atoms colliding with the surface with an energy of 0.07 eV at an angle of 45°, the deviation of the flow of desorbing CD_4 molecules from the normal was 2.4°. For an energy of 0.25 eV and 45°, this value was 4.8°. For hydrogen atoms with an energy of 0.25 eV and the same incident angle, the maximum of methane SDDF should be observed at an angle of 3.6° to the surface normal.

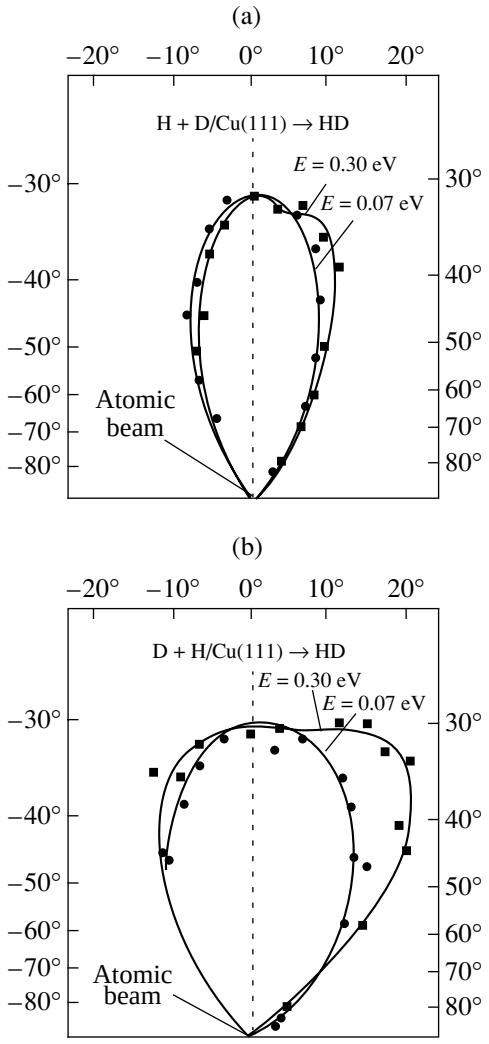

Fig. 36. Spatial distributions of HD molecules formed by the Eley–Rideal mechanism in the reactions (a) $H + D_{ads} \longrightarrow HD$ and (b) $D + H_{ads} \longrightarrow HD$ at T_{surf} = 100 K and two values of beam energies E [16].

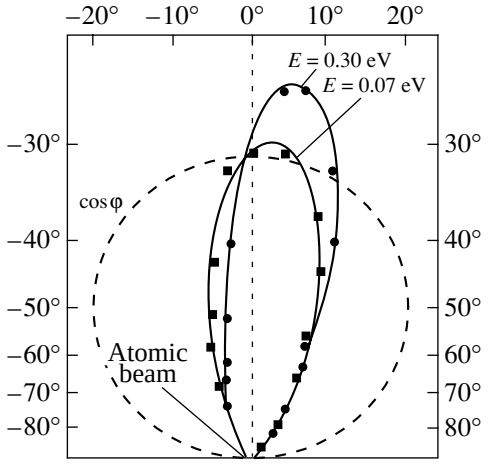

Fig. 37. Spatial distributions of HCl molecules formed in the reaction $H + Cl_{ads} \longrightarrow HCl$ on Au(111) at T_{surf} = 100 K and atomic beam energies of 0.07 and 0.30 eV [6]. The incident beam angle (60°) is shown by an arrow. The dashed circle corresponds to the cosine (Knudsen) distribution.

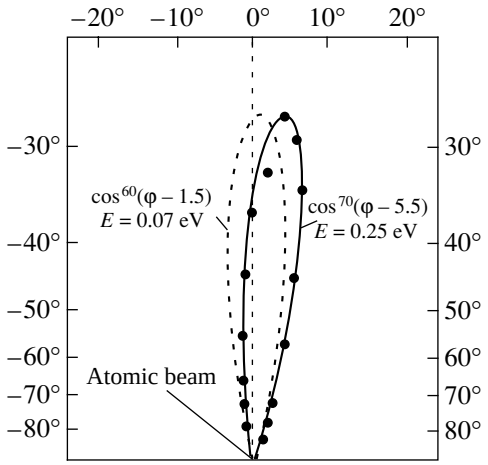

Fig. 38. Spatial distribution of CD_4 molecules formed in the reaction of deuterium atoms (atomic beam) and $\dot{C}D_3$ radicals adsorbed on the Cu(111) surface and at a beam energy of 0.25 eV and T_{surf} = 95 K. The arrow shows the incident beam angle (45°). The solid line corresponds to the function $\cos^{70}(\varphi - 5.5)$. The result obtained at a beam energy of 0.07 eV is shown by the dashed line for comparison [17].

These values agree well with the respective experimental values: 1.5°, 5.5°, and 3.5°.

CONCLUSION

Currently, much information is available on the desorption dynamics of excited molecules that are the products of heterogeneous catalytic reactions. The desorption of translationally excited H_2, N_2, CO_2, and CH_4 was studied in most detail, and their flows and translational energies at different emission angles were measured. There is some correlation between the translational energy of desorbing molecules and the spatial distribution of their flows from the surface.

In the studies of CO oxidation on the stepped surfaces of platinum, palladium, and iridium, anisotropic and inclined spatial distributions of the desorption flows of CO_2 molecules provided radically new information on the active sites where the reaction occurs. The effect of site switching was discovered, i.e., the occurrence of the process on those or other sites of the surface (terraces, steps, trenches, and ridges) depending on the reactant pressure and the surface temperature.

The measurements of SDDF and the velocity distributions of nitrogen molecules in the reactions $NO_{ads} \longrightarrow 1/2N_2 + 1/2O_2$, $N_{ads} + NO_{ads} \longrightarrow N_2 + O_{ads}$,

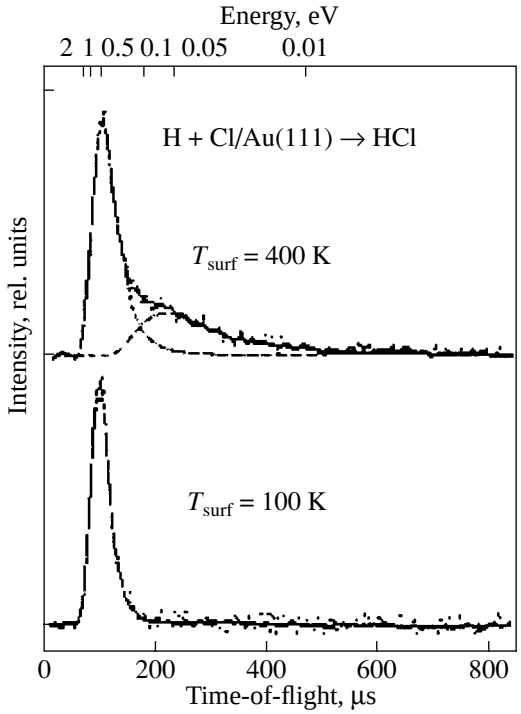

Fig. 39. Time-of-flight distributions of HCl molecules formed by the reaction $H + Cl_{ads} \longrightarrow HCl$ on Au(111) at T_{surf} = 400 and 100 K [6]. The atomic beam angle was 60° relative to the surface normal. The beam energy was 0.07 eV.

$NO_{ads} + CO_{ads} \longrightarrow 1/2N_2 + CO_2$, $N_2O_{ads} \longrightarrow N_2 + O_{ads}$, and $2N_{ads} \longrightarrow N_2$ on Pd(110) provided details on the mechanism of NO decomposition and the emission dynamics of translationally excited N_2 molecules.

A series of studies were carried out on the interaction of atomic beams of hydrogen (H and D) with adsorbed atoms and radicals (H, D, Cl, $CH_3^{\cdot}$, and $CD_3^{\cdot}$). In all cases, the directed desorption of products was observed due to the conservation of momentum parallel to the surface.

The use of modern spectroscopic methods such as LIF, REMI, and EIF made it possible to study the emissions of molecules excited over the internal degrees of freedom. Although there are fewer such data than for translationally excited molecules, they made it possible to obtain the energy distributions of desorbing molecules over the degrees of freedom and determine that $T_{tr} \geq T_{vib} > T_{rot}$.

Unfortunately, there were no measurements of vibrational and rotational excitations of energy levels of molecules desorbing at different angles relatively to the surface. Experiments of this sort would shed light on the details of desorption dynamics and help to construct the corresponding theoretical models.

ACKNOWLEDGMENTS

I thank the Ministry of Education, Science, Sport, and Culture of Japan for financial support in the framework of the 1999–2000 Program for Inviting Foreign Researchers. Support from the Russian Foundation for Basic Research (grant nos. 99-03-32114 and 02-03-33097) is acknowledged. I also thank Professor T. Matsushima for fruitful discussions during the work.

REFERENCES

1. Van Willigen, W., *Phys. Lett. A*, 1968, vol. 28, no. 2, p. 80.
2. Dabiri, A.E., Lee, T.J., and Stickney, R.E., *Surf. Sci.*, 1971, vol. 26, no. 2, p. 522.
3. Becker, C.A., Cowin, J.P., Wharton, L., and Auerbach, D.J., *J. Chem. Phys.*, 1977, vol. 67, no. 7, p. 3394.
4. Comsa, G., David, R., and Schumacher, B.J., *Surf. Sci.*, 1979, vol. 85, no. 1, p. 45.
5. Allers, K.-H., Pfnur, H., Feulner, P., and Menzel, D., *J. Chem. Phys.*, 1994, vol. 100, no. 5, p. 3985.
6. Rettner, C.T., *J. Chem. Phys.*, 1994, vol. 101, no. 2, p. 1529.
7. Matsushima, T., *Heterog. Chem. Rev.*, 1995, vol. 2, no. 1, p. 51.
8. Kislyuk, M.U., Savkin, V.V., Vlasenko, A.G., and Bartan, A.O., *Izv. Akad. Nauk, Ser. Khim.*, 1995, no. 1, p. 30.
9. Colonell, J.I., Gibson, K.D., and Sibener, S.J., *J. Chem. Phys.*, 1996, vol. 104, no. 7, p. 6822.
10. Murphy, M.J., Skelly, J.F., and Hodgson, A., *J. Chem. Phys.*, 1998, vol. 109, no. 9, p. 3619.
11. Balooch, M. and Stickney, R.E., *Surf. Sci.*, 1974, vol. 44, no. 2, p. 310.
12. Balooch, M., Cardillo, M.J., Miller, D.R., and Stickney, R.E., *Surf. Sci.*, 1974, vol. 46, no. 2, p. 358.
13. Steinruck, H.P., Winkler, A., and Rendulic, K.D., *Surf. Sci.*, 1985, vols. 152/153, no. 2, p. 323.
14. Matsushima, T., *J. Chem. Phys.*, 1989, vol. 91, p. 5722.
15. Matsushima, T., *J. Chem. Phys.*, 1990, vol. 93, no. 2, p. 1464.
16. Rettner, C.T. and Auerbach, D.J., *Surf. Sci.*, 1996, vols. 357/358, no. 3, p. 602.
17. Rettner, C.T., Auerbach, D.J., and Lee, J., *J. Chem. Phys.*, 1996, vol. 105, no. 22, p. 10116.
18. Dushman, S., *Scientific Foundations of Vacuum Technique*, Lafferty, J.M., Ed., New York: Willey, 1962, p. 715.
19. Barker, J.A. and Auerbach, D.J., *Surf. Sci. Rep.*, 1985, vol. 4, no. 1, p. 1.
20. Matsushima, T., Matsui, T., and Hashimoto, M., *J. Chem. Phys.*, 1984, vol. 81, no. 11, p. 5151.
21. Matsushima, T., Shobatake, K., Ohno, Y., and Tabayashi, K., *J. Chem. Phys.*, 1992, vol. 97, no. 4, p. 2783.
22. Cao, G., Seymiya, Y., and Matsushima, T., *J. Mol. Catal.*, 1999, vol. 141, no. 1, p. 63.
23. Comsa, G. and David, R., *Surf. Sci. Rep.*, 1985, vol. 5, no. 1, p. 145.
24. Savkin, V.V. and Kislyuk, M.U., *Kin. Katal.*, 1996, vol. 37, no. 4, p. 591.

25. Comsa, G. and David, R., *Chem. Phys. Lett.*, 1977, vol. 49, no. 3, p. 512.
26. Pohelmann, E., Schmitt, M., Hoinkes, H., and Wilsch, H., *Surf. Rev. Lett.*, 1995, vol. 6, no. 3, p. 741.
27. Healey, F., Carter, R., and Hodgson, A., *Surf. Sci.*, 1995, vol. 328, no. 1, p. 67.
28. Comsa, G. and David, R., *Surf. Sci.*, 1982, vol. 117, no. 1, p. 77.
29. Rettner, C.T., Michelsen, H.A., Auerbach, D.J., and Mullins, C.B., *J. Chem. Phys.*, 1991, vol. 94, no. 11, p. 7499.
30. Michelsen, H.A., Rettner, C.T., and Auerbach, D.J., in *A Model System for the Study of Activated Adsorption in Surface Reactions*, Madix R.J., Ed., Berlin: Springer, 1994, vol. 34, p. 185.
31. Kurz, E.A. and Hudson, J.D., *Surf. Sci.*, 1988, vol. 195, no. 1/2, p. 31.
32. Savkin, V.V. and Kislyuk, M.U., *Kinet. Katal.*, 2000, vol. 41, no. 3, p. 453.
33. Palmer, R.L., Smith, J.N., Saltsburg, H., and O'Keffe, D.R., *J. Chem. Phys.*, 1970, vol. 53, no. 5, p. 1666.
34. Bradley, T.L., Dabiri, A.E., and Stickney, R.E., *Surf. Sci.*, 1972, vol. 29, no. 2, p. 590.
35. Steinruck, H.P., Winkler, A., and Rendulic, K.D., *J. Phys. C: Solid State Phys.*, 1985, vols. 152/153, part 1, p. 323.
36. Russel, J.N., Chorkendorff, I., Lanzillotto, A.M., Alvey, M.D., and Yates, J.T., *J. Chem. Phys.*, 1986, vol. 85, no. 10, p. 6186.
37. Allers, K.-H., Pfnur, H., Feulner, P., and Menzel, D., *Surf. Sci.*, 1993, vol. 286, no. 1, p. 297.
38. Comsa, G., David, R., and Schumacher, B.J., *Surf. Sci.*, 1980, vol. 95, no. 1, p. 210.
39. Verheij, L.K., Hugenschmidt, M.B., Anton, A.B., Poelsema, B., and Comsa, G., *Surf. Sci.*, 1989, vol. 210, no. 1/2, p. 1.
40. Lin, T.H. and Somorjai, G.A., *J. Chem. Phys.*, 1984, vol. 81, no. 2, p. 704.
41. Park, Y.-S., Bang, J.-S., and Lee, J., *Surf. Sci.*, 1993, vol. 283, no. 1/2, p. 209.
42. Park, Y.-S., Kim, J.-Y., and Lee, J., *J. Chem. Phys.*, 1993, vol. 98, no. 1, p. 757.
43. Park, Y.-S., Kim, J.-Y., and Lee, J., *J. Chem. Phys.*, 1997, vol. 106, no. 21, p. 8935.
44. Carter, R.N., Murphy, M.J., and Hodgson, A., *Surf. Sci.*, 1997, vol. 387, no. 1, p. 102.
45. Moriwaki, K., Matsumoto, Y., Ikai, M., and Tanaka, K., *Chem. Phys. Lett.*, 1998, vol. 292, no. 2, p. 500.
46. Kislyuk, M.U., Savkin, V.V., and Tret'yakov, I.I., *Kinet. Katal.*, 2000, vol. 41, no. 1, p. 82.
47. Savkin, V.V. and Kislyuk, M.U., *Kinet. Katal.*, 1997, vol. 38, no. 5, p. 793.
48. Savkin, V.V., Bakuleva, T.N., Boeva, O.A., Vlasenko, A.G., Kislyuk, M.U., Sizova, N.N., and Sklyarov, A.V., *Kinet. Katal.*, 1989, vol. 30, no. 6, p. 1455.
49. Murphy, M.J., Skelly, J.F., Hodgson, A., and Hammer, B., *J. Chem. Phys.*, 1999, vol. 110, no. 16, p. 6954.
50. Cosser, R.C., Bare, S.R., Francis, S.M., and King, D.A., *Vacuum*, 1981, vol. 31, p. 503.
51. Campbell, C.T., Ertl, G., Kuipers, H., and Segner, J., *Surf. Sci.*, 1981, vol. 107, no. 1, p. 220.
52. Savkin, V.V., Kislyuk, M.U., and Sklyarov, A.V., *Kinet. Katal.*, 1987, vol. 28, no. 6, p. 1409.
53. Sano, M., Ohno, Y., Yamanaka, T., Matsushima, T., Quinay, E.B., and Jacoby, K., *J. Chem. Phys.*, 1998, vol. 108, no. 24, p. 10231.
54. Matsushima, T., *Z. Phys. Chem.*, vol. 162, p. 1.
55. Kislyuk, M.U., Migulin, V.V., Savkin, V.V., Vlasenko, A.G., Sklyarov, A.V., and Tret'yakov, I.I., *Kinet. Katal.*, 1990, vol. 31, no. 6, p. 1392.
56. Horton, D.R. and Masel, R.I., *Surf. Sci.*, 1983, vol. 125, no. 3, p. 699.
57. Kislyuk, M.U., Migulin, V.V., and Savkin, V.V., *Izv. Akad. Nauk SSSR, Ser. Khim.*, 1994, no. 6, p. 999.
58. Asher, M., Guthric, W.L., Lin, T.H., and Somorjai, G.A., *Phys. Rev. Lett.*, 1982, vol. 49, p. 76.
59. Gibson, K.D., Colonell, J.I., and Sibener, S.J., *Surf. Sci.*, 1999, vol. 443, no. 1, p. 125.
60. Engel, T. and Ertl, G., *J. Chem. Phys.*, 1978, vol. 69, no. 3, p. 1267.
61. Moula, Md.G., Wako, S., Kislyuk, M.U., Ohno, Y., and Matsushima, T., *Stud. Surf. Sci. Catal.*, 2001, vol. 132, p. 701.
62. Matsushima, T. and Asada, H., *Chem. Phys. Lett.*, 1985, vol. 120, nos. 4, 5, p. 412.
63. Matsushima, T. and Asada, H., *J. Chem. Phys.*, 1986, vol. 85, no. 3, p. 1658.
64. Ohno, Y., Matsushima, T., Shobotake, K., and Nozoye, K., *Surf. Sci.*, 1992, vol. 273, no. 2, p. 291.
65. Moula, Md.G., Wako, S., Ohno, Y., Kislyuk, M.U., Kobal, I., and Matsushima, T., *Phys. Chem. Chem. Phys.*, 2000, vol. 2, p. 2773.
66. Palmer, R.L. and Smith, J.N., *J. Chem. Phys.*, 1974, vol. 60, no. 4, p. 1453.
67. Mullins, C.B., Rettner, C.T., and Auerbach, D.J., *J. Chem. Phys.*, 1991, vol. 95, no. 2, p. 864.
68. Matsushima, T., *Surf. Sci.*, 1983, vol. 127, no. 2, p. 403.
69. Segner, J., Campbell, C.T., Doyen, G., and Ert, G., *Surf. Sci.*, 1984, vol. 138, no. 2, p. 505.
70. Pohelmann, E., Schmitt, M., Hoinkes, H., and Wilsch, H., *Surf. Sci.*, 1993, vols. 287/288, nos. 1/2, p. 269.
71. Matsushima, T., *J. Catal.*, 1983, no. 2, p. 446.
72. Colonell, J.I., Gibson, K.D., and Sibener, S.J., *J. Chem. Phys.*, 1995, vol. 103, no. 15, p. 6677.
73. Brown, L.S. and Sibener, S.J., *J. Chem. Phys.*, 1989, vol. 90, no. 5, p. 2807.
74. Matsushima, T. and Ohno, Y., *Catal. Lett.*, 1994, vol. 23, p. 313.
75. Kislyuk, M.U., Savkin, V.V., and Tret'yakov, I.I., *Kinet. Katal.*, 2001, vol. 42, no. 4, p. 594.
76. Ukraintsev, V.A. and Harrison, I., *Surf. Sci.*, 1993, vol. 286, no. 3, p. 571.
77. Kisliuk, P., *J. Phys. Chem. Solids*, 1957, vol. 3, no. 1, p. 95.
78. Kislyuk, M.U. and Bakuleva, T.N., *Izv. Akad. Nauk SSSR, Ser. Khim.*, 1990, no. 12, p. 2699.
79. Matsushita, T., Ohno, Y., and Nagai, K., *J. Chem. Phys.*, 1991, vol. 94, no. 1, p. 704.

80. Ohno, Y., Matsushima, T., and Miki, H., *Surf. Sci.*, 1993, vol. 281, no. 1, p. 234.
81. Ikai, M., Hong, He, Borroni-Bird, C.E., Hirano, H., Tanaka, K., *Surf. Sci.*, 1994, vol. 315, nos. 1/2, p. 973.
82. Ikai, M., Janssen, N.M., Nieuwenhuys, B.E., and Tanaka, K., *J. Chem. Phys.*, 1997, vol. 106, no. 1, p. 311.
83. Cao, G., Moula, Md.G., Ohno, Y., and Matsushima, T., *Surf. Sci.*, 1999, vols. 427/428, nos. 2/3, p. 272.
84. Walker, A.V. and King, D.A., *J. Chem. Phys.*, 2000, vol. 112, no. 3, p. 1938.
85. Cao, G., Moula, Md.G., Ohno, Y., and Matsushima, T., *Phys. Chem. B*, 1999, vol. 103, no. 14, p. 3255.
86. Moula, Md.G., Wako, S., Cao, G., Kimura, K., Ohno, Y., Kobal, I., and Matsushima, T., *Phys. Chem. Chem. Phys.*, 1999, vol. 1, p. 3677.
87. Ikai, M. and Tanaka, K., *J. Phys. Chem. B*, 1999, vol. 103, p. 8277.
88. Ohno, Y., Kimura, K., Bi, M., and Matsushima, T., *J. Chem. Phys.*, 1999, vol. 110, no. 19, p. 8221.
89. Kobal, I. and Matsushima, T., *Trends. Chem. Phys.*, 1999, vol. 7, p. 169.
90. Kobal, I., Kimura, K., Ohno, Y., and Matsushima, T., *Surf. Sci.*, 2000, vol. 445, no. 2, p. 472.
91. Ikai, M. and Tanaka, K., *J. Chem. Phys.*, 1999, vol. 110, no. 17, p. 7031.
92. Matsushima, T., *Chem. Phys. Lett.*, 1989, vol. 155, no. 3, p. 313.
93. Matsushima, T., Shobatake, K., Ohno, Y., and Tabayashi, K., *J. Chem. Phys.*, 1992, vol. 97, no. 4, p. 2783.
94. Matsushima, T., Shobatake, K., and Ohno, Y., *Surf. Sci.*, 1993, vol. 283, no. 1, p. 101.
95. Rzeznicka, I., Ohno, Y., Horino, H., Kobal, I., Kimura, K., and Matsushima, T., *Proc. 9th ICHC*, Varna, Bulgaria, 2000, p. 256.
96. Kimura, K., Ohno, Y., and Matsushima, T., *Surf. Sci.*, 1999, vol. 429, nos. 2/3, p. 455.
97. Wako, S., Moula, Md.G., Cao, G., Kimura, K., Kobal, I., Ohno, Y., and Matsushima, T., *Langmuir*, 2000, vol. 16, no. 9, p. 2689.
98. Moula, Md.G., Mishra, A.B.P., Rzeznicka, I., Kislyuk, M.U., Liu, S., Ohno, Y., and Matsushima, T., *Chem. Phys. Lett.*, 2001, vol. 341, no. 2, p. 225.
99. Rar, A., Sugimura, H., Barrera, A., Ohno, Y., and Matsushima, T., *Surf. Sci.*, 1996, vol. 348, no. 1, p. 77.
100. Stefanov, P.K., Ohno, Y., Yamanaka, T., Seimiya, Y., Kimura, K., and Matsushima, T., *Surf. Sci.*, 1998, vol. 416, no. 1/2, p. 305.
101. Matsushima, T., Akiyama, H., Lesar, A., Sugimura, H., Torre, G.E.D., Yamanaka, T., and Ohno, Y., *Surf. Sci.*, 1997, vol. 386, no. 1, p. 24.
102. Lesar, A., Yamanaka, T., Ohno, Y., and Matsushima, T., *Chem. Phys. Lett.*, 1995, vol. 234, nos. 4–6, p. 330.
103. Yamanaka, T., Moise, C., and Matsushima, T., *J. Chem. Phys.*, 1997, vol. 107, no. 19, p. 8138.
104. Ohno, Y., Sanches, J.R., Lesar, A., Yamanaka, T., and Matsushima, T., *Surf. Sci.*, 1997, vol. 382, no. 1, p. 221.
105. Cao, G., Seimiya, Y., and Matsushima, T., *J. Mol. Catal., A: Chem.*, 1999, vol. 141, no. 1, p. 63.
106. Doen, G., *Vacuum*, 1982, vol. 32, no. 1, p. 91.
107. Polanyi, J.S. and Wong, W.H., *J. Chem. Phys.*, 1969, vol. 51, no. 4, p. 1439.
108. Harris, J. and Andersson, S., *Phys. Rev. Lett.*, 1985, vol. 55, no. 2, p. 1583.
109. Anger, G., Winkler, A., and Rendulic, K.D., *Surf. Sci.*, 1989, vol. 220, no. 1, p. 1.
110. Hayden, B.E. and Lamont, C.L.A., *Chem. Phys. Lett.*, 1989, vol. 160, no. 3, p. 331.
111. Rettner, C.T., Auerbach, D., and Michelsen, H.A., *Phys. Rev. Lett.*, 1992, vol. 68, p. 1164.
112. Rettner, C.T., Michelsen, H.A., and Auerbach, D., *J. Chem. Phys.*, 1995, vol. 102, no. 11, p. 4625.
113. Nielsen, U., Halstead, D., Holloway, S., and Norskov, J.K., *J. Chem. Phys.*, 1990, vol. 93, no. 4, p. 2879.
114. Engdahl, G., Lundqvist, B.I., Nielsen, U., and Norskov, J.K., *Phys. Rev. B. Condens. Matter*, 1992, vol. 45, no. 23, p. 11362.
115. Kurz, E.A. and Hudson, J.D., *J. Vac. Sci. Technol. A*, 1988, vol. 6, part 1, p. 774.
116. Ehrlich, G., *J. Chem. Phys.*, 1959, vol. 31, no. 4, p. 1111.
117. Volter, J., Jungnickel, I., and Rienacker, G., *Z. Anorg. Chem*, 1968, vol. 360, p. 300.
118. Cadenhead, D.A. and Wagner, N.J., *J. Catal.*, 1971, vol. 21, no. 3, p. 312.
119. Alexander, C.S. and Prtchard, J., *J. Chem. Soc., Faraday Trans. 1*, 1972, vol. 68, no. 1, p. 202.
120. Kislyuk, M.U. and Tret'yakov, I.I., *Kinet. Katal.*, 1977, vol. 18, no. 3, p. 550.
121. Gabis, I.E., Kurdyumov, A.A., and Mazaev, S.N., *Poverkhnost.*, 1987, vol. 12, p. 26.
122. Campbell, J.M., Domagala, M.E., and Campbell, C.T., *J. Vac. Sci. Technol., A*, 1991, vol. 9, p. 1693.
123. Kislyuk, M.U., *Surf. Sci.*, 1994, vol. 302, no. 3, p. 395.
124. Kislyuk, M.U., *Kinet. Katal.*, 1999, vol. 40, no. 6, p. 803.
125. Toyoshima, I. and Somorjai, G., *Catal. Rev. – Sci. Eng.*, 1979, vol. 19, no. 1, p. 105.
126. Gibson, K.D., Colonell, J.I., and Sibener, S.J., *Surf. Sci.*, 1995, vol. 343, no. 3, p. 1151.
127. Beutl, M., Lesnik, J., and Rendulic, K.D., *Surf. Sci.*, 1999, vol. 429, no. 1, p. 71.
128. Hamers, R.J., Houston, P.L., and Merrill, R.P., *J. Chem. Phys.*, 1985, vol. 83, no. 11, p. 6045.
129. Smith, J.N. and Palmer, R.L., *J. Chem. Phys.*, 1972, vol. 56, no. 1, p. 13.
130. Gibson, K.D., Colonell, J.I., and Sibener, S.J., *J. Chem. Phys.*, 1995, vol. 103, no. 15, p. 6735.
131. Ikai, M. and Tanaka, K., *Surf. Sci.*, 1996, vols. 357/358, no. 3, p. 781.
132. Hamza, A.V., Stenruck, H.-P., and Madix, R.J., *J. Chem. Phys.*, vol. 86, no. 11, p. 6505.
133. Lee, M.B., Yang, Q.Y., and Ceyer, S.T., *J. Chem. Phys.*, 1987, vol. 87, no. 5, p. 2724.
134. McMaster, M.C. and Madix, R.J., *Surf. Sci.*, 1992, vol. 275, no. 1/2, p. 265.
135. Matsushima, T., Ohno, Y., and Rar, A., *Surf. Sci.*, 1993, vol. 293, no. 1, p. 145.

136. Matsumoto, Y., Okawa, Y., and Tanaka, K., *Surf. Sci.*, 1995, vol. 336, no. 2, p. 762.

137. Ehsasi, M., Matloch, M., Frank, O., Block, J.H., Christmann, K., Rys, F.S., and Hirschwald, W., *J. Chem. Phys.*, 1989, vol. 91, no. 8, p. 4949.

138. Seimiya, Y., Cao, G., Ohno, Y., Yamanaka, T., Matsushima, T., and Jacobi, K., *Surf. Sci.*, 1997, vol. 415, no. 3, p. 988.

139. Kislyuk, M.U., *Kinet. Katal.*, 1998, vol. 39, no. 2, p. 246.

140. Yagi, K., Higashiyama, K., and Fukutani, H., *Surf. Sci.*, 1993, vol. 295, no. 1, p. 230.

141. Takagi, N., Yasui, Y., Sawada, M., Ali, A., Aruga, T., and Nishijima, M., *Chem. Phys. Lett.*, 1995, vol. 232, nos. 5–6, p. 531.

142. Ohno, Y., Matsushima, T., and Uetsuka, H., *J. Chem. Phys.*, 1994, vol. 101, no. 6, p. 5319.

143. Ohno, Y. and Matsushima, T., *Surf. Sci.*, 1995, vol. 341, no. 1/2, p. 172.

144. Mortensen, K., Klink, C., Jensen, F., Besenbacher, F., and Stensgaard, I., *Surf. Sci.*, 1989, vol. 220, nos. 2/3, p. 701.

145. Ladas, S., Siokou, A., Kennou, S., Finnk, T., Imbihl, R., Mertens, F., and Hasse, J., *Surf. Sci.*, 1994, vol. 319, no. 3, p. 337.

146. Schmidt, J., Stuhlmann, Ch., and Ibach, H., *Surf. Sci.*, 1993, vol. 284, no. 1, p. 121.

147. Sowa, E.C., Van Hove, M.A., and Adams, D.L., *Surf. Sci.*, 1988, vol. 199, nos. 1/2, p. 174.

148. Finnis, M.W. and Heine, V., *J. Phys.*, 1974, vol. 4, p. 37.

149. Murphy, M.J. and Hodgson, A., *Surf. Sci.*, 1996, vol. 368, no. 1, p. 55.

150. Kubiak, G.D., Sitz, G.O., and Zare, R.N., *J. Chem. Phys.*, 1984, vol. 81, no. 12, p. 6397.

151. Uetsuka, H., Watanabe, K., and Kunimori, K., *Surf. Sci.*, 1996, vol. 363, no. 1, p. 73.

152. Uetsuka, H., Watanabe, K., Ohnuma, H., and Kunimori, K., *Surf. Sci.*, 1997, vols. 377–379, no. 3, p. 765.

153. Uetsuka, H., Watanabe, K., Ohnuma, H., and Kunimori, K., *Surf. Rev. Lett.*, 1997, vol. 4, p. 1359.